Tropical Stationary Wave Response to ENSO: Diabatic Heating Influence on the Indian Summer Monsoon

YOUKYOUNG JANG*

Center for Ocean–Land–Atmosphere Studies, Calverton, Maryland

DAVID M. STRAUS

Department of Atmospheric, Oceanic and Earth Sciences, George Mason University, Fairfax, and Center for Ocean–Land–Atmosphere Studies, Calverton, Maryland

(Manuscript received 1 February 2012, in final form 5 June 2012)

ABSTRACT

The atmospheric response to boreal summer tropical diabatic heating is studied in the atmospheric model component of the Community Atmosphere Model [CAM, version 3 (CAM3)] of the National Center for Atmospheric Research. An idealized heating function (with broad vertical but localized horizontal structure) is *added* to CAM3 near the equator; the circulation response is studied as a function of the sign of the heating and its longitude (Indian Ocean to eastern Pacific Ocean). The atmospheric circulation forced by the added heating interacts with all the physical and dynamical processes in CAM3; the total heating is the sum of the added heating and that produced by CAM3. In experiments using climatological sea surface temperature, added cooling (heating) over the Maritime Continent induces asymmetric anticyclonic (cyclonic) circulation extending toward India, opposing (reinforcing) the climatological monsoon flow and weakening (strengthening) the Indian monsoon. The anchoring of the anticyclonic (cyclonic) circulation over India as the added cooling (heating) is moved eastward over warm SST regions is greatly reduced when a slab ocean model is used. A negative (positive) air–sea feedback over the Indian Ocean is identified when heating (cooling) is added in the Indonesian region. Experiments in which the total heating is similar to estimates of the observed heating for the summer of 1987 are examined.

1. Introduction

One central theme in the study of seasonal predictability is the influence of persistent tropical sea surface temperature (SST) anomalies on both the tropical and extratropical circulations. A tropical SST anomaly (assumed positive) tends to increase both low-level convergence and moisture (Lindzen and Nigam 1987; Raymond 1994), thereby promoting anomalous deep convection and hence diabatic heating. The heating is balanced by anomalies in rising motion (in the time mean), which in turn is balanced at upper levels by increased divergence. The divergence, in turn, interacts with the mean flow to produce the Rossby wave source that determines the far-field barotropic response (Sardeshmukh and Hoskins 1988). Within the tropics, the anomalous heating (and associated rising motion) produces both stationary Kelvin waves to the east and Rossby waves to the west, as described in the simple model of Gill (1980).

The relationship of the seasonal mean Indian monsoon to the state of the eastern Pacific SST related to El Niño–Southern Oscillation (ENSO) is a problem of some importance that involves the tropical response to heating. In particular, a negative correlation between seasonal mean (June–September) eastern Pacific SST and seasonal mean monsoon rainfall has been noted, so that summers of warm events (El Niños) are associated with deficient rainfall (Kumar et al. 1999; Palmer et al. 1992; Straus and Krishnamurthy 2007). However, in recent years ENSO has seemingly lost its impact on the Indian summer monsoon (Kumar et al. 1999; Kripalani

* Current affiliation: Department of Earth and Environment, Florida International University, Miami, Florida.

Corresponding author address: Youkyoung Jang, Department of Earth and Environment, Florida International University, 11200 SW 8th St., Miami, FL 33199.
E-mail: yjang@cola.iges.org

DOI: 10.1175/JAS-D-12-036.1

and Kulkarni 1997; Kirtman and Shukla 2000; Mokhov et al. 2011). For example, the strong El Niño in 1997 was accompanied by a normal monsoon, not a drought as expected.

Troup (1965) showed that India is typically located near a node (zero contour) in the pressure pattern associated with El Niño, well away from the regions of anomaly extrema (such as the sinking branch of the anomalous Walker circulation over the Maritime Continent). In addition, Troup (1965) and Webster et al. (1998) noted that small displacements of the node would place India in either weak positive or weak negative pressure related to the long-term summer average. Slingo and Annamalai (2000) also suggested that subtle shifts in the domain of influence of ENSO can lead to differing responses of the monsoon. These considerations indicate that knowledge of the details of the anomalous SST or diabatic heating associated with a particular El Niño or La Niña event is necessary to understand the monsoon response.

The tropical response to diabatic heating is also affected by air–sea coupling, especially in the monsoon regions. The experiments of Wu and Kirtman (2005) and Fu et al. (2002) showed that inclusion of regional air–sea coupling over the Asian monsoon region improved the simulation of the variability of the Asian monsoon rainfall. In the regions of large mean rainfall, prescribing SST in a numerical model leads to excess precipitation, whereas atmospheric negative feedback to changes in SST leads to a reduced rainfall response in an atmosphere–ocean coupled model, and to more realistic variability of the monsoon. Wang et al. (2003) also showed that the anomalous circulation induced by descending motion in the Maritime Continent is closely linked to air–sea interaction.

As a first step in understanding the ENSO–monsoon relationship, this paper seeks to understand the dynamics of the tropical boreal summer response to idealized anomalous diabatic heating. In particular, we want to complete the following goals:

1) Determine the sensitivity of the tropical circulation to the location of anomalous (tropical) heating anomalies that have idealized broad vertical and localized horizontal structures, within the context of the ENSO–monsoon interaction problem. Our approach is analogous to that used by Barsugli and Sardeshmukh (2002, hereafter BS), who studied the sensitivity to the location of tropical SST anomalies.
2) Determine the effect of air–sea coupling on this sensitivity.

From a modeling perspective, there are several approaches available to achieve these goals:

1) Run a full atmospheric general circulation model (AGCM) with both normal and anomalous SST.
2) Build an idealized general circulation model (GCM) and force it with specified diabatic heating.
3) Modify an existing GCM (either atmosphere only or coupled) so that relatively small *changes* in diabatic heating are added to the model.

In the first option, one has no control over the diabatic heating, since differences in convective parameterizations may lead to very different modeled diabatic heating anomalies for the same SST. In the second option, one has complete control over the diabatic heating but at the expense of completely losing the feedback of the dynamics on the heating.

We explore the third option in this paper in the context of the Community Atmosphere Model, version 3 (CAM3). This idea is to specify idealized changes in the diabatic heating (e.g., due to ENSO), yet retain the full feedback of the dynamics on the heating in the context of the full model. For example, the vertical motion induced by the added heating will change the divergence and vorticity fields throughout the tropics, leading to changes in the moist and radiative heating fields produced by the model's parameterizations. In reality, cumulus convection (diabatic heating in the model) is coupled with the circulation and can interact with the large-scale dynamics (Watanabe and Jin 2003).

The approach of specifying additional heating anomalies circumvents the uncertainty in the model diabatic heating response to SST or wind stress, and has been used previously by Meehl et al. (2008) and Lappen and Schumacher (2012). The ultimate cause of the anomalous heating (e.g., SST or wind stress anomalies) is not accessible by this method, which requires knowledge of either the real or idealized diabatic heating. Estimates of observed diabatic heating rely on the reanalysis circulation and temperature fields (since the heating is obtained from the thermodynamic equation), and so are subject to some uncertainty, especially in data-poor regions.

In this paper, however, we concentrate for the most part on idealized heating configurations. This will provide some insight into whether the responses to complex heating distributions may be estimated as linear combinations of the idealized responses derived in this paper. This approach is analogous to the estimates of the dynamical Green's function estimated, for example, in Branstator (1985), or the response to idealized SST anomalies studied by BS.

To take into account air–sea coupling in the monsoon regions, we also run experiments with the AGCM coupled to a slab ocean model (hereafter SOM). In Jang and

Straus (2012), the same approach is used in numerical experiments in which the diabatic heating diagnosed from observations is used to understand the varied monsoon circulation and rainfall responses in different observed El Niño summers.

In section 2, data used in this study are described. Section 3 gives the characteristics of observed diabatic heating and wind during El Niño summer. In section 4, we briefly describe the method, including the generation of some very idealized heating profiles and details of experiments in this study. In section 5, the results of forced experiments and the role of air–sea interaction are shown. Section 6 gives a summary of this study.

2. Data

We use wind data from the 40-yr European Centre for Medium-Range Weather Forecasts (ECMWF) Re-Analysis (ERA-40) and diabatic heating from the Chan and Nigam (2009) diagnosis of the ERA-40. Both datasets extend from 1000 to 100 hPa. Precipitation data are obtained from the National Oceanic and Atmospheric Administration (NOAA) Climate Prediction Center (CPC) Merged Analysis of Precipitation (CMAP) (Xie and Arkin 1997). The streamfunction, velocity potential, rotational wind, and divergent wind fields are calculated from the wind data. The SST data are obtained from the NOAA Optimum Interpolation (OI) Sea Surface Temperature (Reynolds et al. 2002). The outgoing longwave radiation (OLR) data are from the National Center for Atmospheric Research (NCAR) with gaps filled with temporal and spatial interpolation. All datasets are monthly; we use a summer mean from May through August. The ERA-40 dataset extends from 1957 to 2002, and the CMAP data extend from 1979 to 2007. The period that we use here is from 1979 to 2002. The three-dimensional diabatic heating (Chan and Nigam 2009; Nigam et al. 2000) is diagnosed as a residual in the thermodynamic equation using the analyzed vertical velocity [quasi-diabatic heating (QDB)].

3. Diabatic heating and wind during El Niño summer

The composite characteristics of observed mean SST, diabatic heating (QDB), OLR, precipitation, and wind anomalies for May–August of El Niño are shown in Figs. 1 and 2 (the 5 yr since 1979 with the largest values of the Niño-3.4 index during May–August are selected for compositing: 1982, 1987, 1991, 1994, and 1997). Both SST and diabatic heating show positive anomalies over the central Pacific (Figs. 1a,b). Weak negative SST anomalies appear over the western Pacific (Fig. 1a), although the negative anomalies of the diabatic heating over the western Pacific (Fig. 1b) have comparable magnitudes to the positive anomalies over the central Pacific. In addition, OLR and precipitation show weakening of convection over the western Pacific and eastern Indian Ocean during El Niño summer (Figs. 1c,d). The comparable La Niña composite is roughly the mirror image of the El Niño composite, with relatively weak positive over the Maritime Continent.

The velocity potential and divergent wind fields at 200 hPa are shown for the El Niño summer composite in Fig. 2b. Anomalous upper-level convergent wind and positive velocity potential anomalies over the western Pacific and eastern Indian Ocean imply downward motion, while divergent wind and negative velocity potential anomalies over the central Pacific imply upward motion.

The anomalous streamfunction and rotational wind fields at 850 hPa consist of a pair of anticyclones extending from the western Pacific to the Indian region, along with a pair of anomalous cyclonic centers over the central Pacific (Fig. 2a). The low-level easterly anomalies seen in Fig. 2a act to weaken the climatological southwesterlies over the Arabian Sea shown in Fig. 2c, thus reducing moisture transport over India.

4. Experiments

a. Model

The version of the NCAR CAM3 used here as the AGCM has 26 vertical levels and a 42-wave triangular spectral truncation. The formulation of the physics and dynamics of CAM3 is detailed by Collins et al. (2006). A spectral Eulerian formulation is used to resolve dynamical motions along with a semi-Lagrangian transport scheme for dealing with the large-scale transport of water and chemical species. CAM3 also includes the Community Land Model, version 3, for the treatment of land surface energy exchanges; the land model is integrated on the same horizontal grid as CAM3.

An SOM will be used for regional air–sea coupling. The ocean model coupled to the AGCM is a simple thermodynamic slab mixed-layer model, which is a part of the NCAR CAM3 modeling system. The depth of the mixed-layer is fixed to a climatological annual cycle with a 200-m cap. At each grid point, the AGCM supplies the heat flux to the ocean model, and the ocean model returns the SST to the AGCM. The SST evolves according to the heat flux given by the AGCM. The coupling will be allowed in only the Indian Ocean and western Pacific (30°S–20°N, 60°–150°E). In the

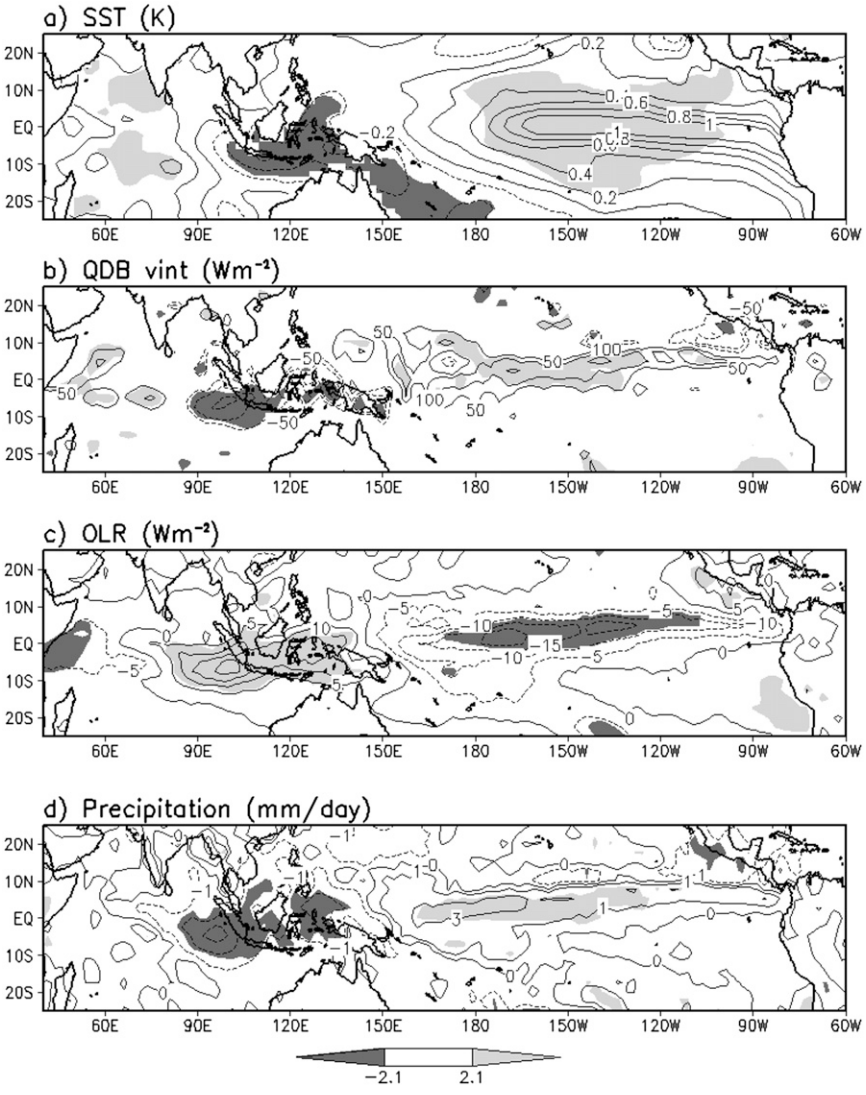

FIG. 1. El Niño composite of anomalies during summer (May–August) for (a) SST (K), (b) diabatic heating vertically integrated from the surface to 100 hPa (W m^{-2}), (c) outgoing longwave (W m^{-2}), and (d) precipitation (mm day^{-1}). Shading is 5% significance values.

other ocean basins, prescribed climatologically varying monthly SST was used as a boundary condition for the AGCM.

b. Control runs

Two control simulations, each 21 yr long, were run. One control simulation (CCTL) uses prescribed, climatologically varying SSTS in all oceans. The second control simulation (CTL SOM) uses this SST field only outside the Indian and western Pacific oceans, where it is coupled to the SOM. The prescribed SST has only a climatological annual cycle; the effect of interannual variability of the Pacific SST field is not introduced. The two control runs are used as a basis for comparison with the forced experiments. In the latter, ENSO-related effects are introduced through the structure of the added heating.

c. Forced runs

1) METHOD

Two sets of forced experiments were carried out. One set uses the climatological SST field as a boundary condition over all oceans; the second set is coupled to the SOM as described above. In each set, 20 seasonal integrations (May–August) were performed using the 20 initial conditions from 1 May from each year of the appropriate control run. Each simulation is run through

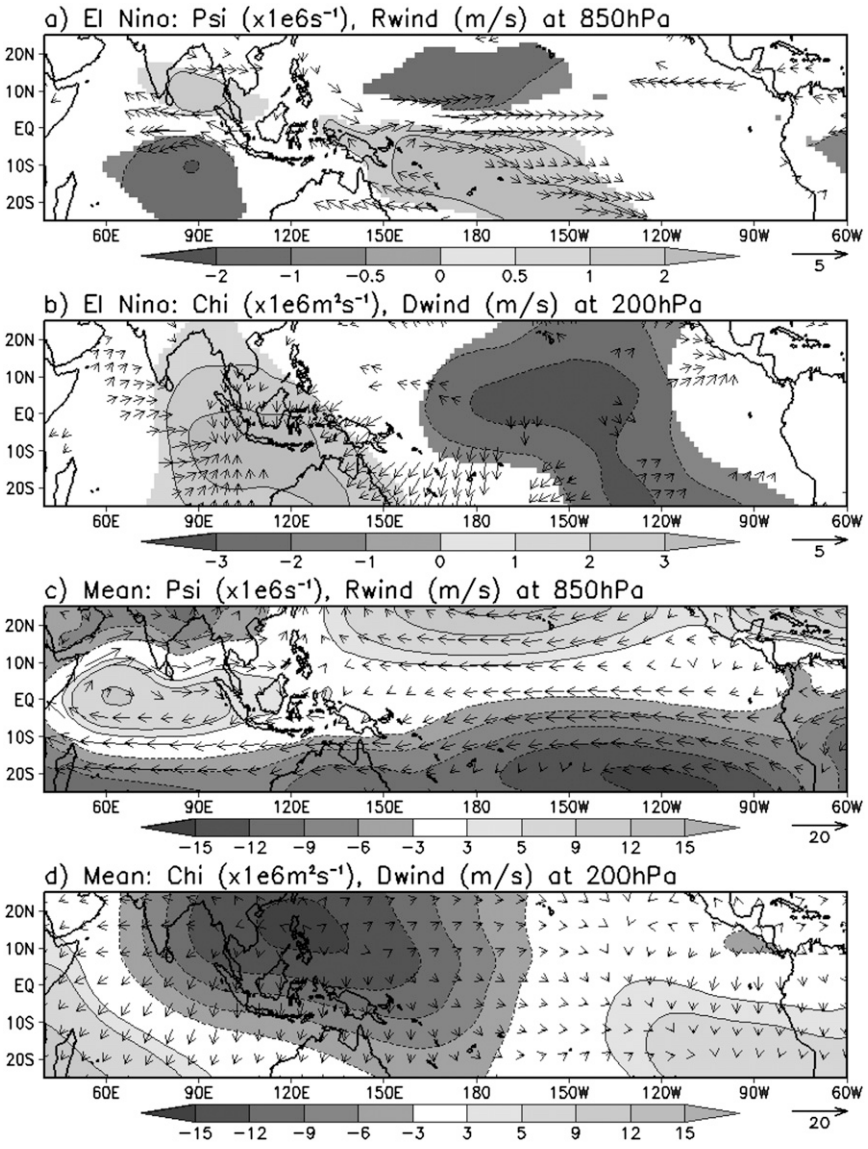

FIG. 2. El Niño composite of anomalies during summer (May–August) for (a) streamfunction (shading, $\times 10^6$ s^{-1}) and rotational wind (vector, m s^{-1}) at 850 hPa, and (b) velocity potential (shading, $\times 10^6$ m^2 s^{-1}) and divergent wind (m s^{-1}) at 200 hPa. Shadings and vectors are only shown at the 5% significance level. Climatological mean of May–August for (c) streamfunction ($\times 10^6$ s^{-1}) and rotational wind (m s^{-1}) at 850 hPa, and (d) velocity potential ($\times 10^6$ m^2 s^{-1}) and divergent wind (m s^{-1}) at 200 hPa.

August, and the 20-run ensemble average of the May–August seasonal means is compared to the corresponding ensemble seasonal mean from the corresponding control simulation. This ensemble procedure is expected to reduce the effect of midlatitude disturbances in particular and internal variability in general, and we can expect the ensemble mean model response to be dominated by forced waves from tropical heating or cooling. There is one caveat, however: while the added heating is the same in each of the 20 integrations, the changes in the AGCM's own diabatic heating induced by the additional forcing (the GCM effect) will not necessarily be the same in each of the 20 integrations. The role of internal variability is taken into account in a simple way through the use of the *t* statistic to assess the difference in all ensemble seasonal means shown.

2) FORCED EXPERIMENTS

In these experiments, a heating with an idealized vertical profile (given in appendix A) is added to the

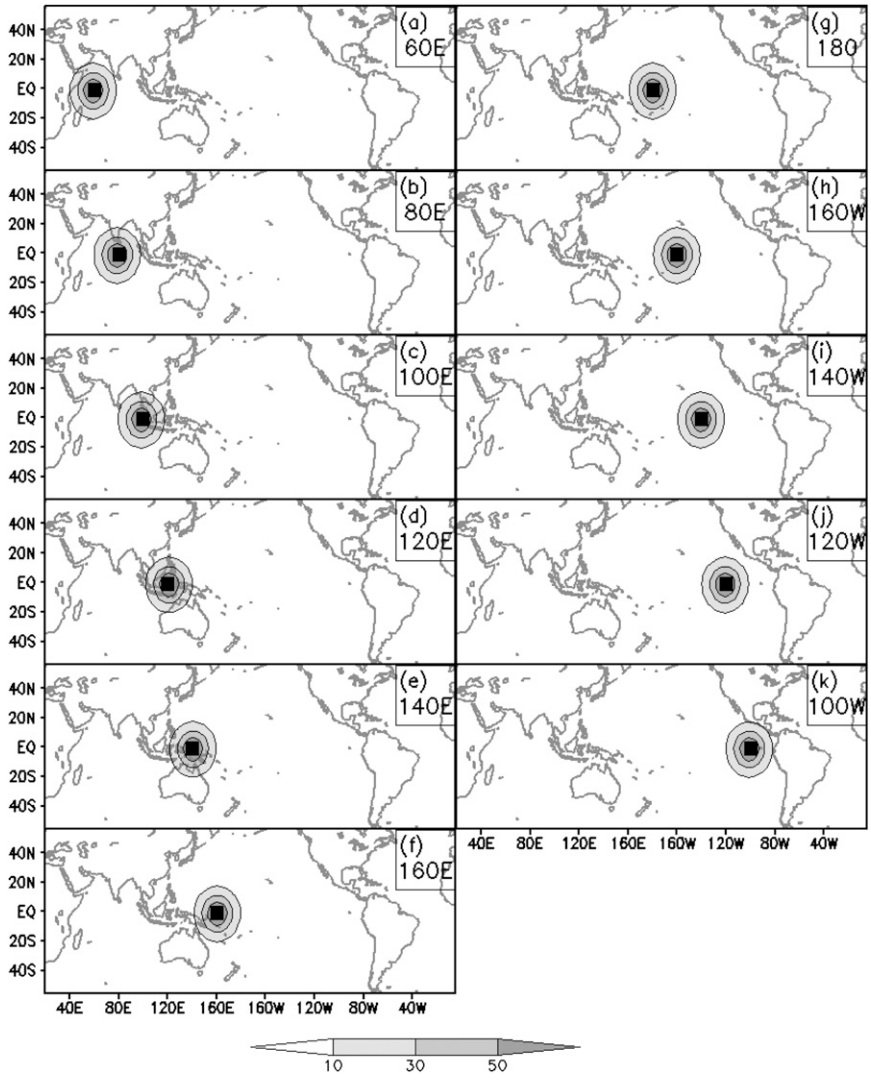

FIG. 3. Positive diabatic forcing is integrated vertically from the surface to 100 hPa (W m^{-2}). Maximum of the forcing is +1 K day^{-1}. Each forcing is centered at (a) 60°, (b) 80°, (c) 100°, (d) 120°, (e) 140°, and (f) 160°E; (g) 180°; and (h) 160°, (i) 140°, (j) 120°, and (k) 100°W. Black dots show the center of the forcing.

temperature tendency equation of CAM3. In the horizontal, the heating assumes an isotropic Gaussian form with an *e*-folding distance corresponding to 20°; the center of the Gaussian distribution is located near the equator (1.4°S) and at a particular longitude. The following four types of experiments were carried out:

1) Sensitivity to longitudinal locations of forcing: The longitudes of the center of the additional heating varied from 60°E to 100°W with a 20° interval. The latitudinal location of the forcing is near the equator (1.4°S) as shown in Fig. 3. Experiments were run with both positive and negative heating. Climatological SSTs are used globally.
2) Sensitivity to latitudinal locations of forcing: The cooling is located at 7°S, 1.4°S (the standard), and 7°N. Climatological SSTs are used globally. Although experiments for all longitudes were performed, we report in detail only the results for one case, in which the heating is placed at 120°E.
3) Role of air–sea interaction: Heating or cooling is inserted at 120°E using the AGCM coupled to the regional SOM. Results are compared to the equivalent forced run in type 1 using prescribed SST. Although SOM experiments were carried out at all longitudes, we report only on those at 120°E.
4) Observed diabatic heating for the boreal summer of 1987 event: This summer was associated with both an

El Niño event and a dry Indian monsoon. Note that the diabatic heating composite of El Niño summer (Fig. 1b) does not have a significant signal over India because it includes three El Niños (1991, 1994, and 1997) with either a wet or a normal monsoon.

5. Results of forced experiments

a. Warm ocean (Indian Ocean and western Pacific) forcing

1) COUPLED DYNAMICAL CONVECTIVE RESPONSE

One can think of added localized heating (cooling) over the western Pacific in the forced experiments as appropriate for a La Niña (El Niño). The composite negative diabatic heating anomalies seen in observed El Niño events in this region are shown in Fig. 1. The maximum diabatic cooling is seen at 120°E, thus motivating us to focus first on the idealized case of cooling inserted at 120°E with prescribed SST over the globe (non-SOM). The results show both local anomalous downward motion and compensating upward motion (negative omega) appear over the Indian Ocean, as seen in Fig. 4c. In contrast, the vertical motion in a simple dry model consists of a single downward branch of the Walker circulation (Watanabe and Jin 2003). In the present experiments, the interaction between convection and large-scale dynamics creates additional vertical motion in regions remote from the forcing.

The response of the divergent meridional wind (local Hadley circulation) at 850 hPa is shown in Fig. 4b. In the forcing region, there are positive wind anomalies to the north of the cooling and negative anomalies to the south, corresponding to low-level divergence, consistent with the descending motion. Over the equatorial Indian Ocean, however, the wind anomalies correspond to low-level convergence, related to ascending motion (Fig. 4c). The equatorial Indian Ocean is a strong convective region during the northern summer (shown as strong negative omega in Fig. 4d), so that anomalous ascending motion strengthens the convection, leading to positive anomalies of diabatic heating over the equatorial Indian Ocean (Fig. 5a).

Here we address the issue of the modification of the direct response to the added heating by the moist process and radiative processes in the AGCM. This diabatic heating feedback consists of the sum of heating rates due to moist processes (convection and resolved condensation) and radiation (longwave and shortwave). The anomalous heating rate due to moist processes shown in Fig. 5c has all the features of the total diabatic heating response, with comparable magnitudes (Fig. 5a). The longwave response shown in Fig. 5d has a magnitude of roughly 20 W m^{-2} in the forcing region, compared to a magnitude of roughly 100 W m^{-2} for the total diabatic heating (Fig. 5a). The sign of the longwave heating response in the forcing region is consistent with weakened convection and less trapping of longwave energy. The shortwave heating rate anomalies are quite small compared to those of the other processes (not shown).

The heating and precipitation responses to the additional cooling have local components (negative anomalies over the forcing region) but also remote responses (negative over India, positive over the equatorial Indian Ocean, Bay of Bengal, and Philippine Sea in Figs. 5a,b). The positive responses over the Bay of Bengal and Philippine Sea agree with Annamalai (2010), who studied the response to anomalous cold SST over the Indonesian Sea in a moist linear baroclinic model (Fig. 6e in that paper). In contrast, the negative response over India does not appear in Annamalai (2010). This study uses forcing that is more spatially extended, which might lead to a strong nonlinearity in the response. Alternatively, the difference between the response in this study and that of Annamalai (2010) may be due to differences in the basic state. These remote heating responses over India are mediated by the circulation response (see below) and thus represent the feedback of dynamics on heating.

The anomalies of streamfunction and rotational wind fields at 850 hPa shown in Fig. 5e can be understood in terms of a simple Gill response (Gill 1980): one pair of anticyclonic circulations to the west of the cooling (Rossby wave response) and a Kelvin wave response to the east of the forcing. The anomalous easterlies within the anticyclonic circulation near India oppose the climatological westerlies over the Arabian Sea adjacent to India (Fig. 5f), thus weakening convection and diabatic heating over India.

To mimic the La Niña–like upward motion over the Maritime Continent, the idealized heating is inserted at 140°E. We chose this longitude because the responses to the forcing here are relatively strong and clear compared to the 120°E case. The center of the local response in the diabatic heating (Fig. 6a) appears somewhat to the north of the center of the inserted forcing (at 1.4°S). The precipitation (Fig. 6b) and lower-level divergence field (integrated from the surface to 800 hPa, shown in Fig. 6d) also show a displacement to the north of the center of the forcing, although the lower-level divergence is more complicated. In contrast, the upper-level divergence fields (integrated from 275 to 80 hPa) show positive anomalies centered at 1.4°S, although shifted slightly to the west (Fig. 6c). Since the meridional

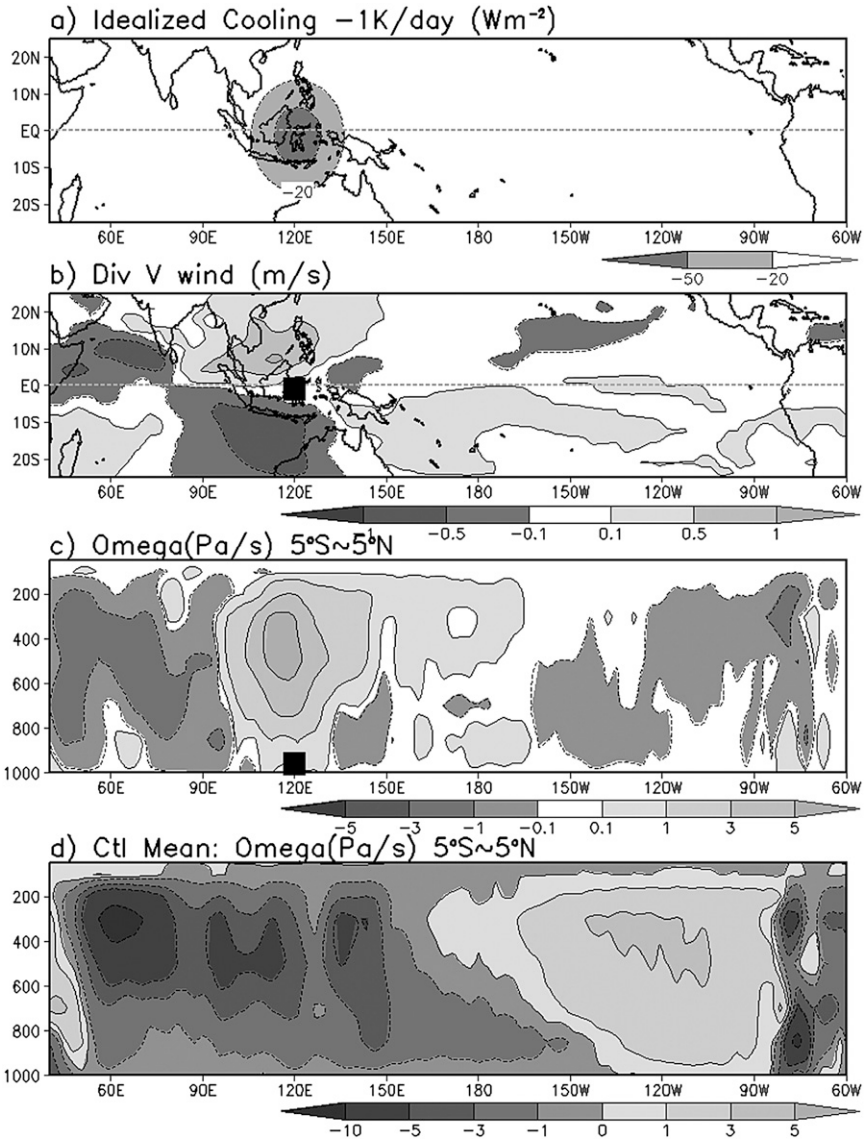

FIG. 4. (a) Inserted idealized cooling (W m^{-2}) is integrated from the surface to 100 hPa and the maximum is 1 K day^{-1} (non-SOM experiment). (b) At the surface, divergent meridional wind response to the idealized cooling (m s^{-1}). (c) Vertical structure of the omega (averaged from 5°S to 5°N) response to the idealized cooling (Pa s^{-1}). (d) Control mean of the vertical structure of omega averaged from 5°S to 5°N. In (b) and (c), only the 5% significance values are shaded. Black dots show the center of the cooling.

displacement is limited to the lower troposphere, we suggest that it is related to the boundary layer and/or other low-level moist processes.

Following the evolution of the response, it was observed that 1 day after the heating is turned on, a low in the surface pressure appears, centered at the forcing region, along with surface convergence. As time evolves, two cyclonic circulations develop slightly to the west of the forcing, consistent with centers of low pressure to the north and south of the forcing region. The surface convergence consistent with these lows induces moisture convergence and leads to the off-center additional heating response mentioned above.

Consistent with our results, Wang et al. (2003) found that the Rossby response to tropical heating in a dry simple model is not symmetric about the equator during the northern summer. The asymmetry is attributed in Wang et al. (2003) to the strong easterly vertical wind shear over the Indian Ocean region. In this study using a full AGCM, the streamfunction (Fig. 6e) and vorticity

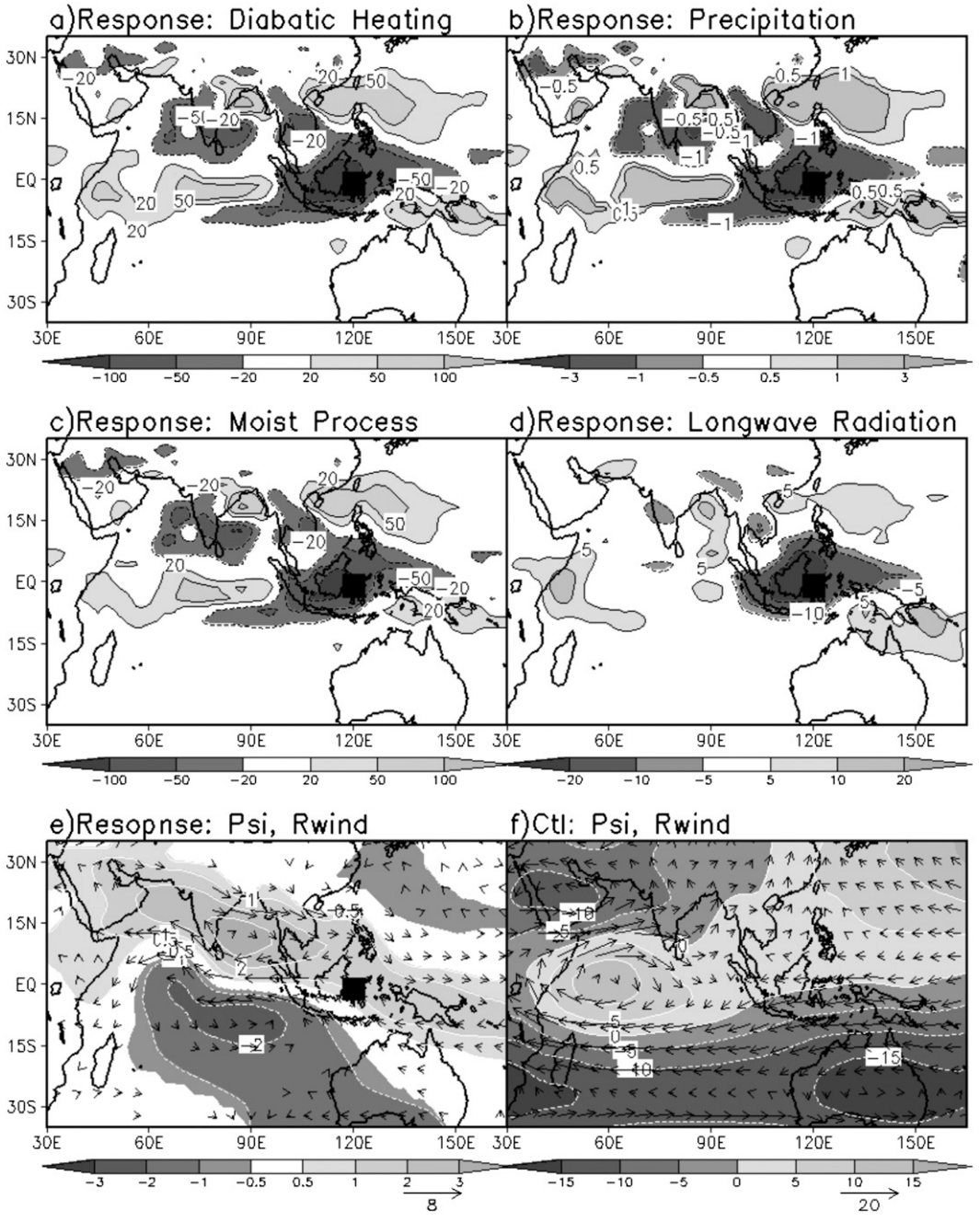

FIG. 5. Response to idealized cooling at 120°E (non-SOM experiment). (a) Diabatic heating vertically integrated from the surface to 100 hPa (W m^{-2}), (b) precipitation (mm day^{-1}), (c) heating rates by moist process (W m^{-2}), (d) longwave radiation (W m^{-2}), (e) streamfunction ($\times 10^6$ s^{-1}) and rotational wind (m s^{-1}) at 850 hPa, and (f) mean streamfunction and rotational wind from the control run. Values at 5% significance are selected and shaded from (a) to (e). Black dots show the center of the cooling.

(Fig. 6f) also show a generally strengthened response to the north of the equator. This asymmetry of the atmospheric circulation response in the full AGCM induces further asymmetry in the diabatic heating and precipitation response.

2) SENSITIVITY TO LONGITUDE

Figure 7 shows the diabatic heating anomalies in both heating and cooling experiments for a variety of forcing locations over the warm ocean (Indian Ocean and

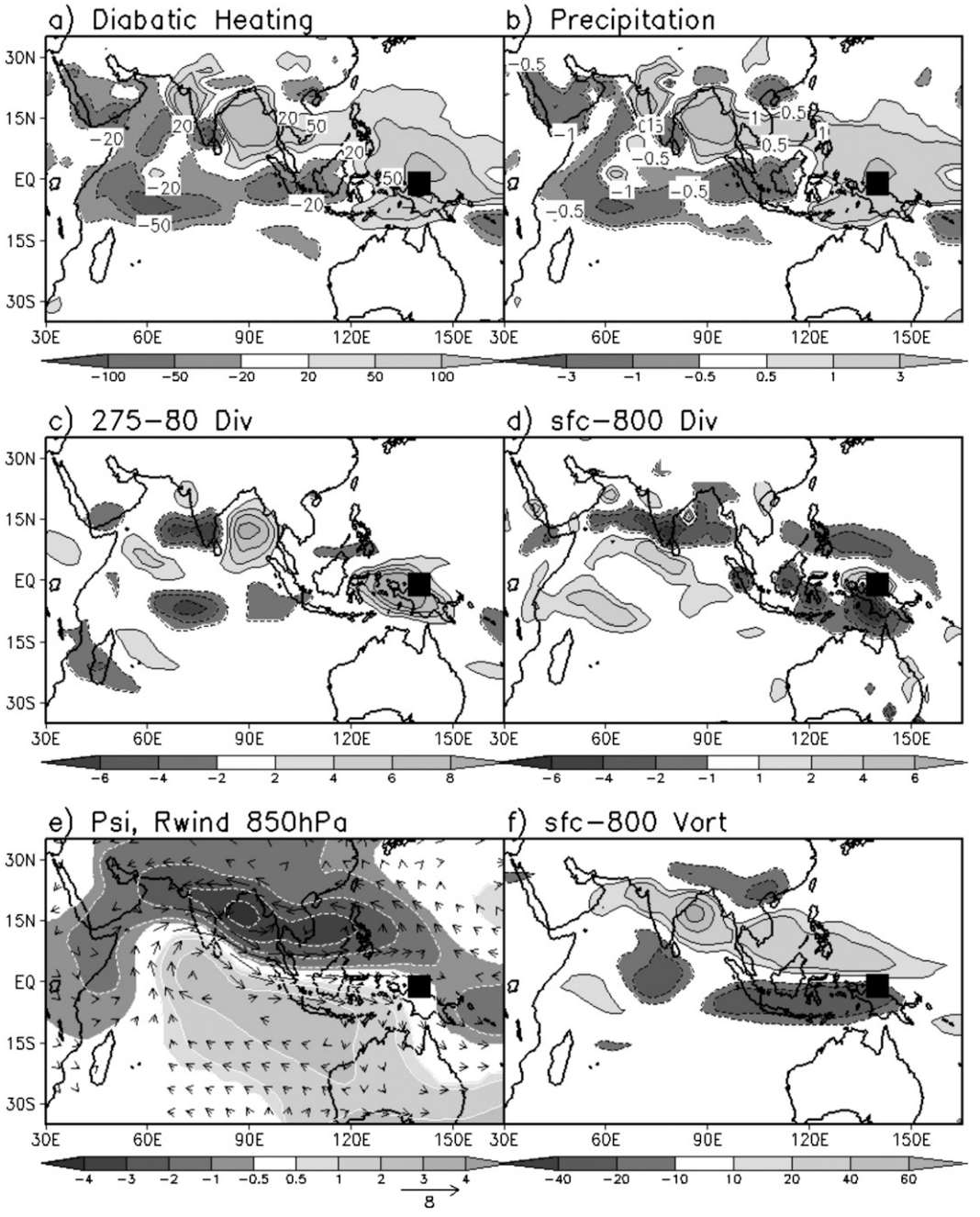

FIG. 6. Response to idealized heating inserted at 140°E (non-SOM experiment). (a) Vertically integrated diabatic heating (W m^{-2}), (b) precipitation (mm day^{-1}) (c) divergence integrated from 275 to 80 hPa ($\times 10^{-3}$ kg m^{-2} s^{-1}), (d) divergence integrated from surface to 800 hPa ($\times 10^{-3}$ kg m^{-2} s^{-1}), (e) streamfunction ($\times 10^{6}$ s^{-1}) and rotational wind (m s^{-1}) at 850 hPa, and (f) vorticity from the surface to 800 hPa ($\times 10^{-3}$ kg m^{-2} s^{-1}). Only statistically significant values at 5% are selected and shaded. Black dots show the center of the heating.

western Pacific). Figure 8 shows the corresponding 850-hPa streamfunction, and Fig. 9 shows sections of the equatorial vertical velocity (omega). There are significant local responses for each forcing as well as remote responses in the vicinity of India. For the heating experiments, a meridionally extended local diabatic heating is seen for a range of forcing longitudes (Figs. 7c–f).

When the heating is at 100°, 120°, 140°, and 160°E, strong positive anomalies of the diabatic heating are

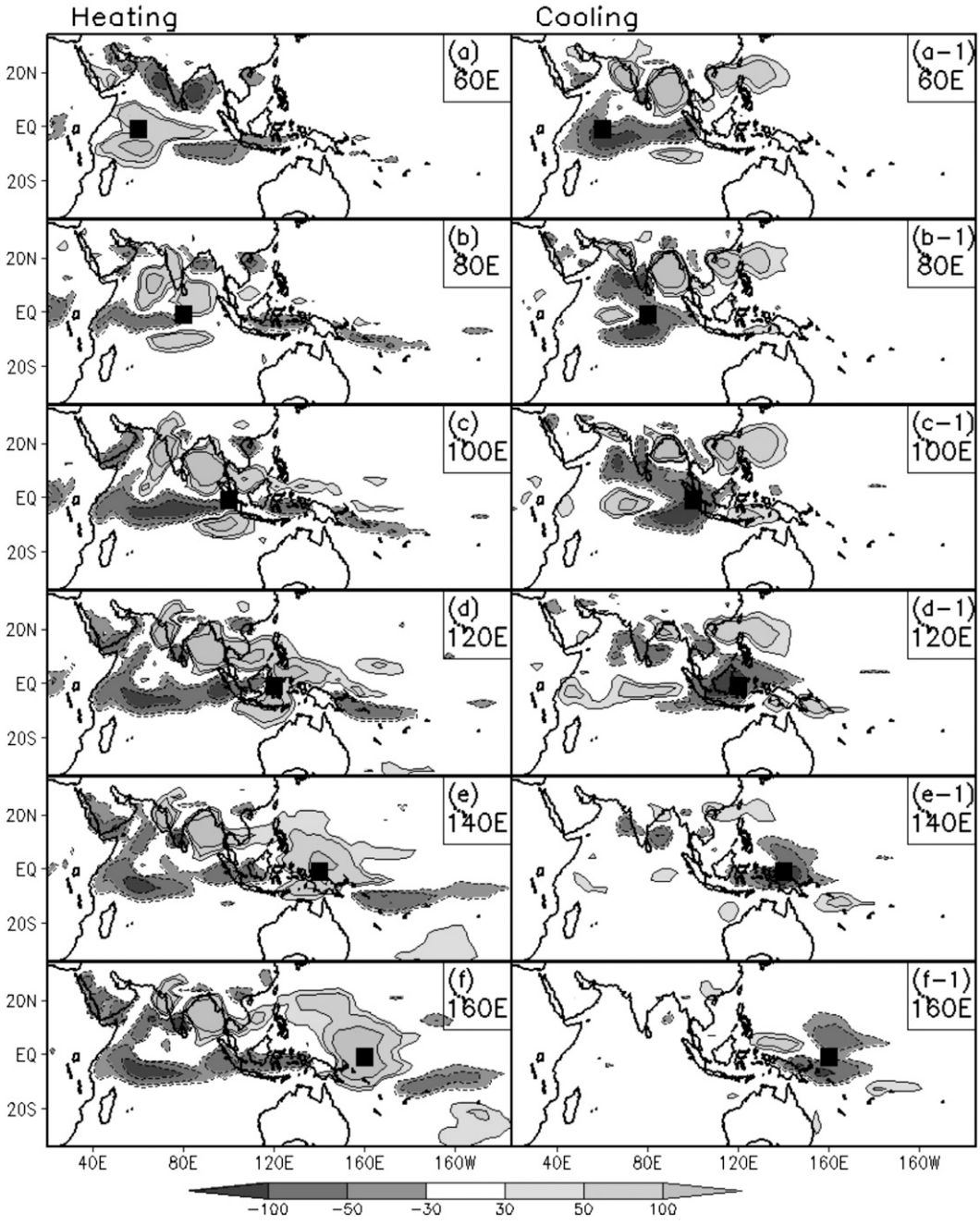

FIG. 7. Diabatic heating response to inserted forcing (non-SOM experiment). Response to (a)–(f) heating and (a-1)–(f-1) cooling. Diabatic heating is integrated vertically from the surface to 100 hPa (W m^{-2}). Maximum of the forcing is +1 K day^{-1} heating and −1 K day^{-1} cooling. Each forcing is centered at (a),(a-1) 60°, (b),(b-1) 80°, (c),(c-1) 100°, (d),(d-1) 120°, (e),(e-1) 140°, and (f),(f-1) 160°E. Only statistically significant values at 5% are selected and shaded. Black dots show the center of each forcing.

consistently seen on both eastern and western sides of India, regardless of the location of the forcing. The anomalous westerlies over the Arabian Sea associated with the cyclonic circulations response strengthen the low-level westerly wind, while the increased wind-induced evaporation over the warm ocean leads to increased latent heat flux to the atmosphere. This positive latent heat flux (not shown here) reinforces the diabatic heating in the vicinity of India.

Note that since the SST is prescribed in these experiments, the ocean temperature does not respond to the loss of the energy due to positive latent heat flux

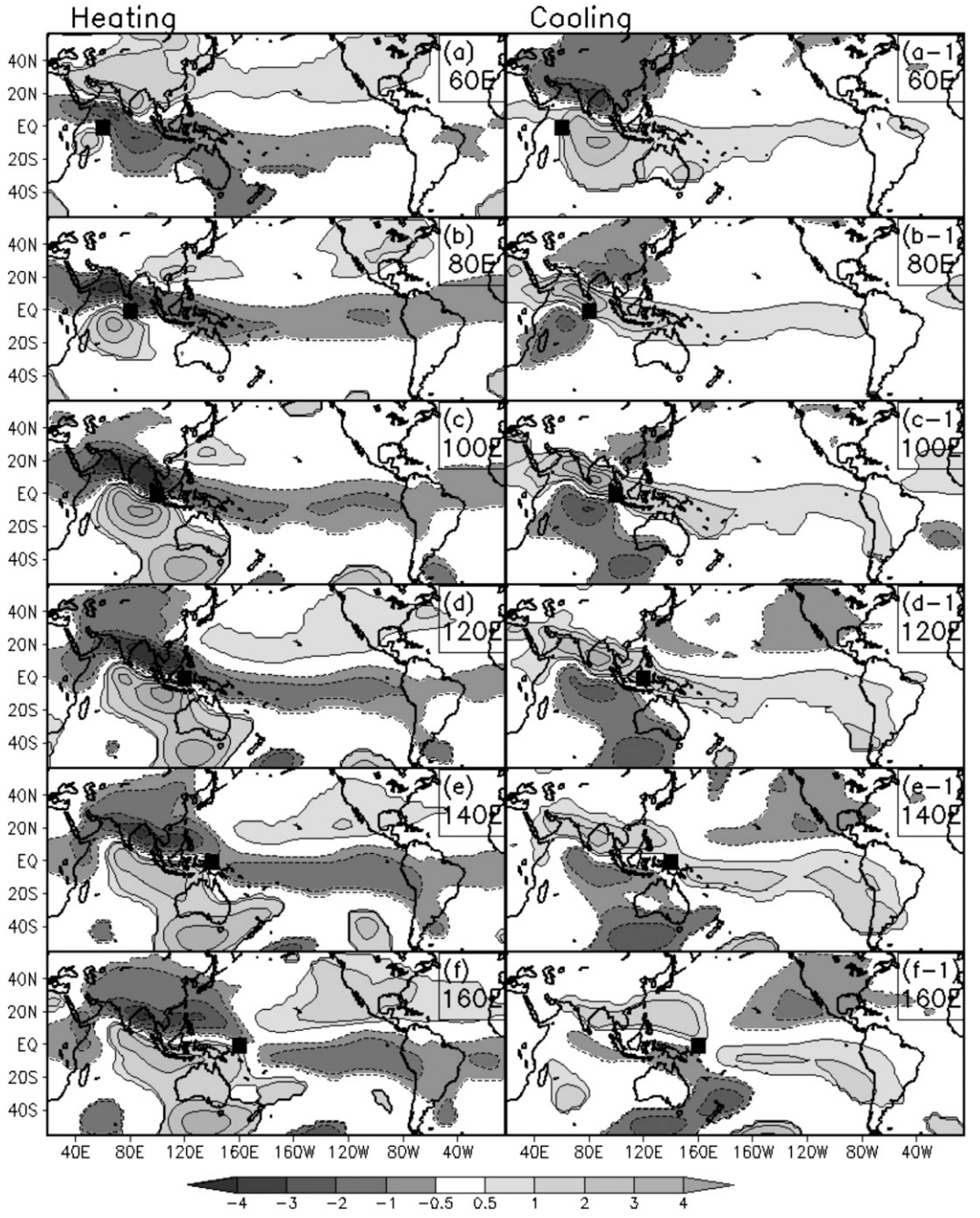

FIG. 8. Streamfunction (at 850 hPa) response ($\times 10^6$ s^{-1}) to inserted forcing (non-SOM experiment). Response to (a)–(f) heating and (a-1)–(f-1) cooling. Each forcing is centered at (a),(a-1) 60°, (b),(b-1) 80°, (c),(c-1) 100°, (d),(d-1) 120°, (e),(e-1) 140°, and (f),(f-1) 160°E. Only statistically significant values at 5% are selected and shaded. Black dots show the center of each forcing.

anomalies, leading to an exaggeration of the diabatic heating. Air–sea interaction effects are discussed in the next section.

In the cooling experiments (right panels of Fig. 7), negative anomalies of diabatic heating appear over India for forcing in the ~100°–160°E range. In Annamalai (2010), anomalously negative SST over the equatorial eastern Indian Ocean (in the region of the cooling at 100°E in this study) leads to a strengthened monsoon trough with positive precipitation anomalies over India and the Bay of Bengal. The corresponding positive anomalies in terms of the diabatic heating are only seen

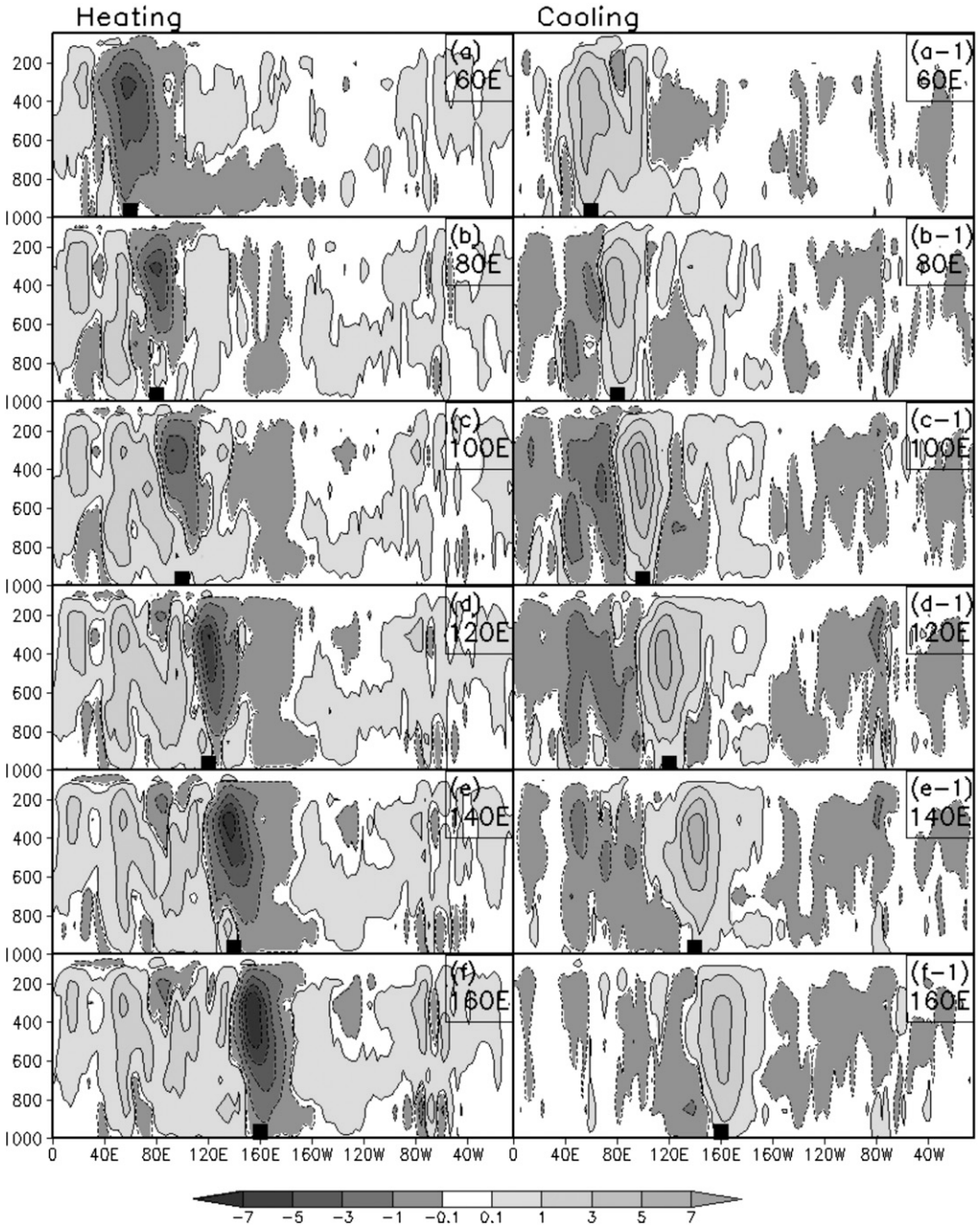

FIG. 9. Vertical structure of omega responses (Pa s^{-1}) to (a)–(f) heating and (a-1)–(f-1) cooling (non-SOM experiment). Response is averaged between 5°S and 5°N. Each forcing is centered at (a),(a-1) 60°, (b),(b-1) 80°, (c),(c-1) 100°, (d),(d-1) 120°, (e),(e-1) 140°, and (f),(f-1) 160°E. Values at 5% significance are selected and shaded. Black dots show the center of each forcing.

in the northern Bay of Bengal and the Philippine Sea in the case of the cooling at 60°, 80°, 100°, and 120°E.

The negative anomalies of diabatic heating over India and the Bay of Bengal in the cooling experiments are relatively weak compared to the response to the heating experiments. Anomalous easterlies as a part of the induced anticyclonic circulation weaken the monsoon flow (Fig. 5e and right panels of Fig. 8). In the vicinity of the Indian region, the weakened winds lead to less transfer of latent heat from the ocean to the atmosphere, contributing to the asymmetry of the remote response in the total diabatic heating near India between the heating

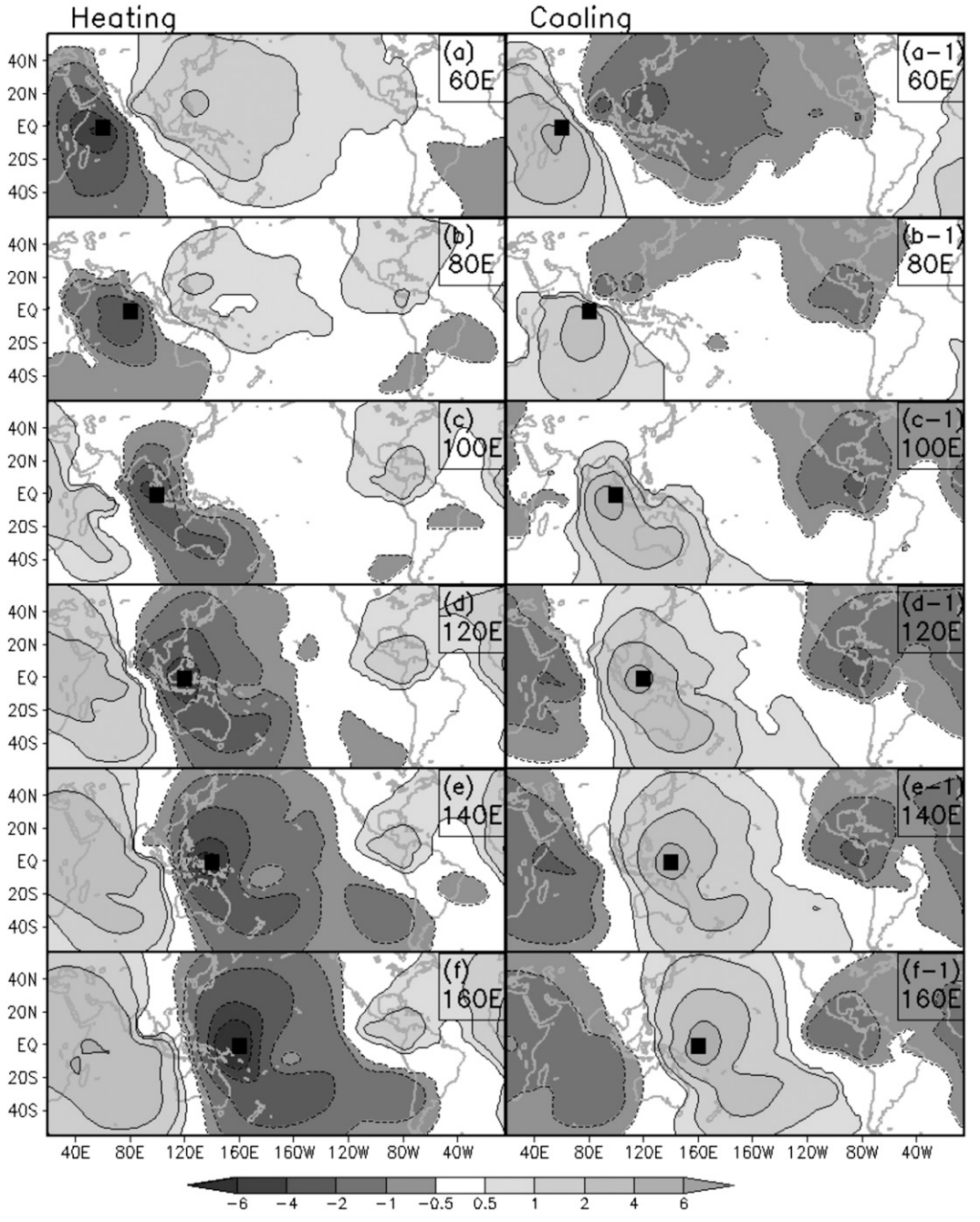

FIG. 10. As in Fig. 8, but for velocity potential (at 200 hPa) response ($\times 10^6$ m^2 s^{-1}).

and cooling experiments. However, the climatology over these areas in the control run has systematic errors, such as weak wind and precipitation, compared to the observation (mentioned in appendix B). Thus, the response related to the latent heat might include the effect of the systematic errors.

With the cooling inserted at 120°E (Fig. 4), we have previously shown anomalous downward vertical motion in the forcing region along with upward motion over the equatorial Indian Ocean. This behavior is also seen when the cooling is introduced over a wide range of longitudes in terms of omega and velocity potential at 200 hPa (right panels of Figs. 9 and 10). For heating, the opposite pattern of vertical motion is seen (left panels of Fig. 9). This compensating vertical motion has been also shown in a moist baroclinic model (Watanabe and Jin

2003). In addition, the control run has strong precipitation along the Somalia coast, and it might influence the strong compensating response to the heating over the Maritime Continent.

The positive velocity potential response to the cooling indicates anomalous downward motion as suppressing convection. In the case of the cooling over the tropical western Pacific (El Niño–like), the anomalous downward motion does not reach India (Figs. 10d-1,e-1), and this implies that a simple cooling over the western Pacific may not directly lead to the anomalous downward motion over India that is related to depressed precipitation, possibly explaining certain warm events associated with a normal monsoon. Further, the cooling alone over the western Pacific might not be enough to explain the full influence of El Niño on the monsoon. This will be discussed again in the section about observed diabatic heating forcing experiment (section 5d).

The responses of the 850-hPa streamfunction to the heating experiments in the left panels of Fig. 8 show a common response: a Rossby response (a pair of cyclonic circulations) to the west of the forcing and a Kelvin response to the east of the forcing. This forced Rossby wave response is also seen in AGCM experiments with El Niño–related SST forcing (Keshavamurthy 1982; Lau and Nath 2000). Depending on the location of the forcing, however, there are some variation in the magnitudes and spatial patterns. For forcing located from 80° to 160°E, we note the consistent westward expansion of the Rossby wave response, leading to a circulation that appears to be anchored over the Indian region. This is accompanied by similar anchored responses in the diabatic heating (Fig. 7). The circulation response in general consists of the direct response to the forcing and the response to the additional diabatic heating over the Indian region.

The diabatic heating response to the heating is stronger over the Indian monsoon region than the cooling response (Fig. 7). However, we have found that with the SOM, the magnitude of the diabatic heating response over the warm ocean regions is similar between the heating and cooling experiments, and this result holds for all longitudes of the idealized forcing. The prescribed SST in the heating experiments does not allow the ocean to cool via the release of the latent heat flux from the ocean, and thus it leads to an exaggerated response over the Indian region. This excessive response does not tend to occur in the cooling experiments.

3) SENSITIVITY TO LATITUDE

Figure 11 presents experiments in which cooling is inserted at 120°E with three latitudinal locations: 7°S, the equator (1.4°S), and 7°S [results from heating at latitude 1.4°N (not shown) are very similar to those at 1.4°S]. With the cooling at 7°S, the anomalously negative diabatic heating anomalies in the southern Bay of Bengal and India that are seen in the standard case (cooling at 1.4°S) weaken and almost disappear (Figs. 11b,c). Positive heating anomalies still remain in the northern Bay of Bengal. The response of the surface wind consists of easterlies over the southern India and the equatorial western Indian Ocean in Figs. 11a–c. When the cooling is at 7°S (Fig. 11c), the easterlies over southern India weaken, consistent with the weakened circulation (Fig. 11f). A simple explanation is that the weakening of the local response over India is due to an increased meridional displacement of the forcing region from India. In contrast, the anchoring effect (westward extension of the Rossby wave response) seems to be robust.

b. Cold ocean (central and eastern Pacific) forcing

When the forcing is over the cold ocean (the central and eastern Pacific), the responses of diabatic heating and atmospheric circulation are relatively weak compared to those of the forcing over the warm ocean discussed in the previous subsection. The diabatic heating responses produced by the AGCM's parameterizations (not shown) have very weak remote components, particularly over India.

Figure 12 shows the vertical structure of the response of the divergence fields, and also the diabatic heating response, for the 140°W forcing experiments. The divergence fields integrated from the surface to 800 hPa show only one center in the immediate forcing region, with convergence (divergence) seen in the heating (cooling) experiments in Fig. 12c (Fig. 12d). In the 275–80-hPa divergence fields, however, the divergence field shows two centers displaced from the forcing location (Figs. 12e,f).

The two anomalous upper-level divergence (convergence) centers seen in Fig. 12e (Fig. 12f) are partly aligned with the two low-level cyclonic (anticyclonic) centers in the classic Gill response seen in Fig. 13c (Fig. 13c-1). The upper-level divergence (convergence) induces anomalous upward (downward) motion, reinforcing the diabatic heating (cooling). The horizontal structure of the upper-level divergence is similar to that of the diabatic heating response in both cases. In summary, the vertical structure of the local response is quite distinct from the response to forcing over warmer oceans.

The vertical section of omega averaged between 5°S and 5°N for forcing at 180° shows local and remote responses over the Indian Ocean, similar to those seen in the previous section (not shown). However, when the forcing is over the cold ocean east of 180°, no compensating motion over the Indian Ocean is seen for

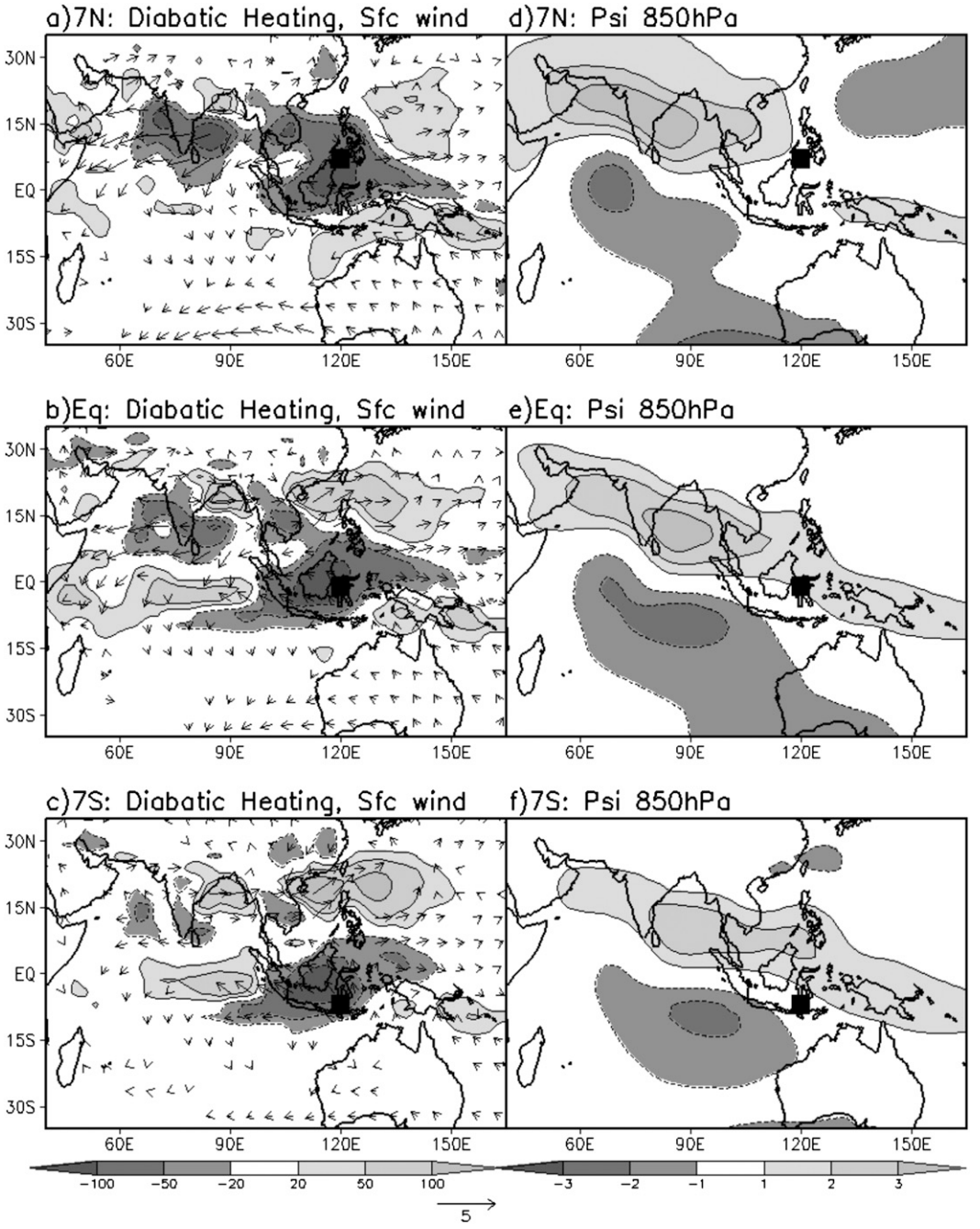

FIG. 11. Response of wind (m s^{-1}) at the surface and diabatic heating (shading) vertically integrated from the surface to 100 hPa (W m^{-2}) to the forcing (cooling) at 120°E (non-SOM experiment): cooling at (a) 7°N, (b) the equator, and (c) 7°S. Response of streamfunction ($\times 10^6$ s^{-1}) at 850 hPa to the forcing at 120°E: cooling at (d) 7°N, (e) the equator, and (f) 7°S. Values at 5% significance are selected and plotted as shading and vectors. Black dots show the center of the forcing.

either heating or cooling experiments (not shown). The magnitude of the response is similar in both heating and cooling experiments.

Figure 13 shows the 850-hPa streamfunction fields for forcing over the cold SST. Here, the magnitudes of the Rossby response are generally similar for both heating and cooling experiments, unlike the results obtained for forcing over the warm SST. However, the Kelvin-like response to the east of the forcing has propagated eastward into the southern equatorial Indian ocean in

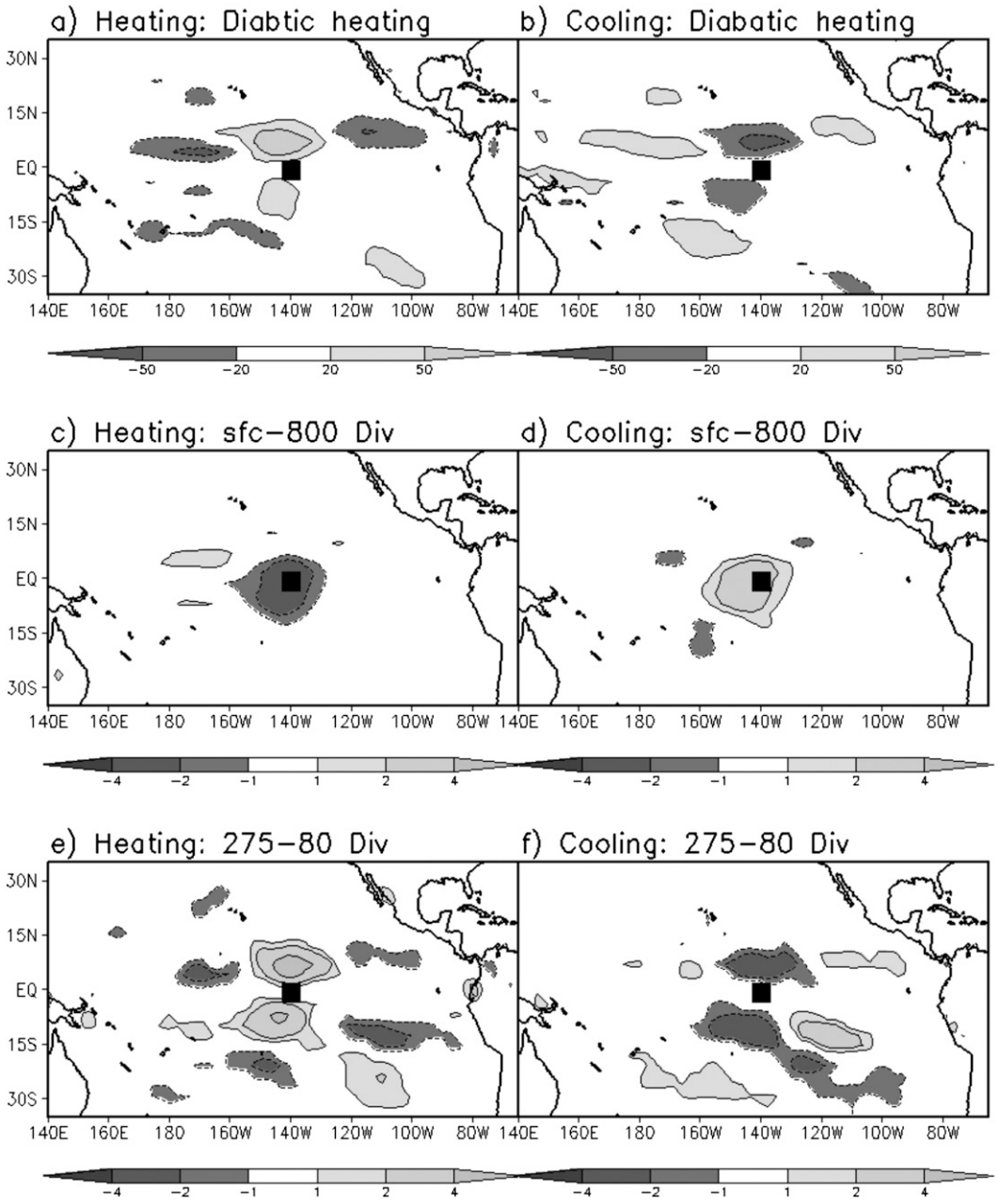

FIG. 12. Response to the forcing centered at 140°W (non-SOM experiment) for the (a),(c),(e) heating and (b),(d),(f) cooling experiments. (a),(b) Diabatic heating response (W m^{-2}). (c),(d) Divergence fields integrated from the surface to 800 hPa ($\times 10^{-3}$ kg m^{-2} s^{-1}). (e),(f) Divergence fields integrated from the 275 to 80 hPa ($\times 10^{-3}$ kg m^{-2} s^{-1}). Values at 5% significance are selected and shaded. Black dots show the center of the forcing.

the heating experiments (Figs. 13c–e), but it does not appear in the cooling experiments. The cooling (heating) over the eastern Pacific can be considered as a part of La Niña (El Niño) forcing. The eastward propagation of the Kelvin response seen only with El Niño forcing indicates a source of asymmetry in the response to El Niño and La Niña. In Pillai and Annamalai (2012), the Kelvin wave–related response over the Indian Ocean is also simulated in an AGCM with wide tropical Pacific SST anomalies, for both warm and cold events. Lin et al. (2007) shows that the Kelvin wave response to El Niño forcing penetrates into the Indian region more strongly in a dry simple model than one by La Niña forcing, which is related to an easterly mean flow.

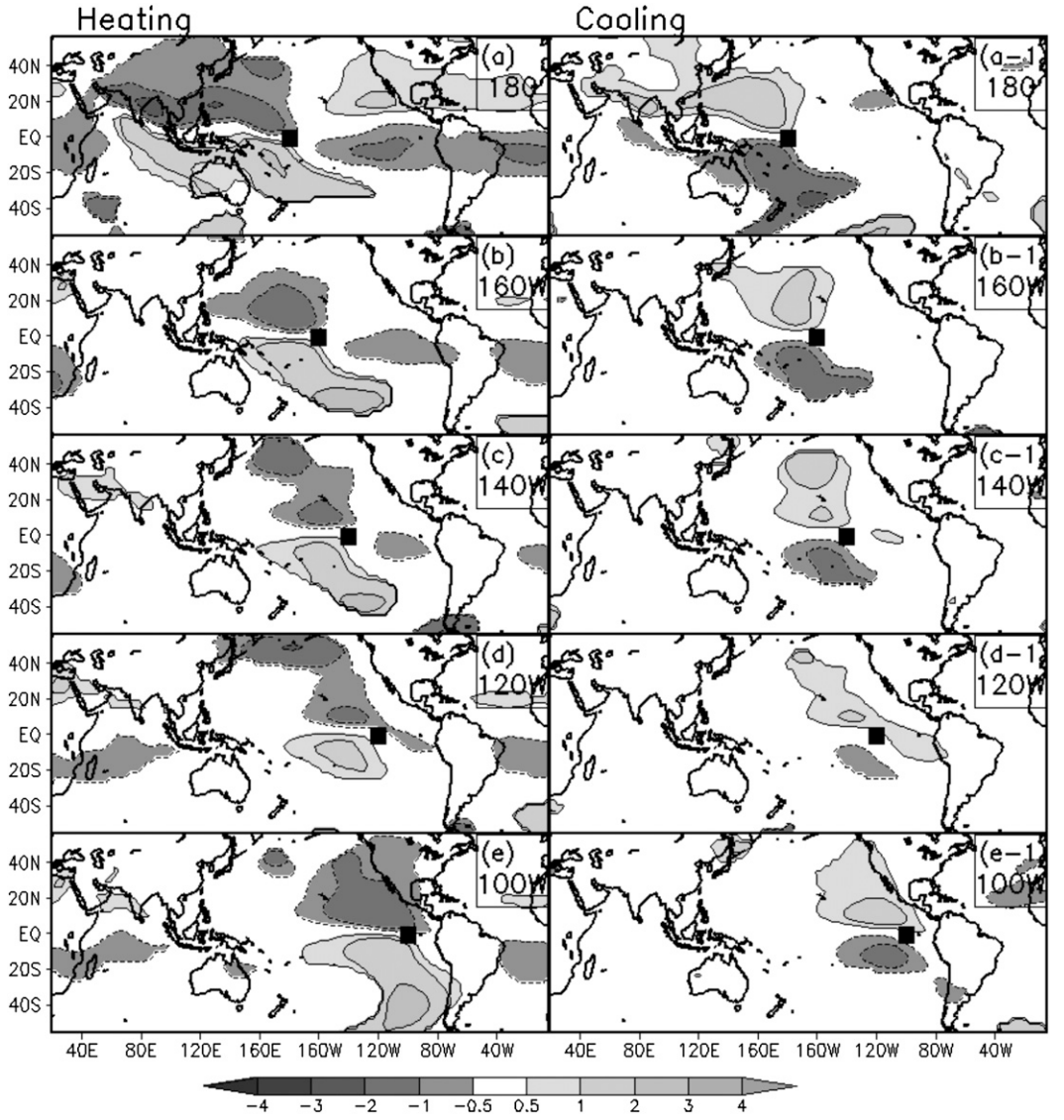

FIG. 13. Streamfunction at 850-hPa response ($\times 10^6$ s^{-1}) to inserted forcing (non-SOM experiment). Response to (a)–(e) heating and (a-1)–(e-1) cooling. Each forcing is centered at (a),(a-1) 180° and (b),(b-1) 160°, (c),(c-1) 140°, (d),(d-1) 120°, and (e),(e-1) 100°W. Only statistically significant values at 5% are selected and shaded. Black dots show the center of each forcing.

c. Air–sea interaction

1) HEATING EXPERIMENT

The SOM is applied over the Indian Ocean and western Pacific in experiments with the same idealized forcing as in the previous section. The responses to idealized heating centered at 120°E with the SOM experiments are compared with the non-SOM experiments in Fig. 14. Applying air–sea coupling leads to the weakening of negative diabatic heating anomalies over the equatorial Indian Ocean and the disappearance of the positive anomalies over the Arabian Sea near India (cf. Figs. 14a,b). The significant positive latent heat flux over the Arabian Sea in the vicinity of India in Fig. 14e also does not appear in the SOM experiments in Fig. 14f. This is consistent with the appearance of negative SST anomalies in this region (Fig. 14g).

Our interpretation of the reduced SST anomalies in the SOM-forced experiment is that the ocean-to-air latent heat flux anomalies due to increased wind speeds over the Arabian Sea (seen clearly in the non-SOM experiments) cool the ocean, thus constituting a negative feedback.

In Figs. 14c,d, the responses of streamfunction at 850 hPa are shown for both non-SOM and SOM

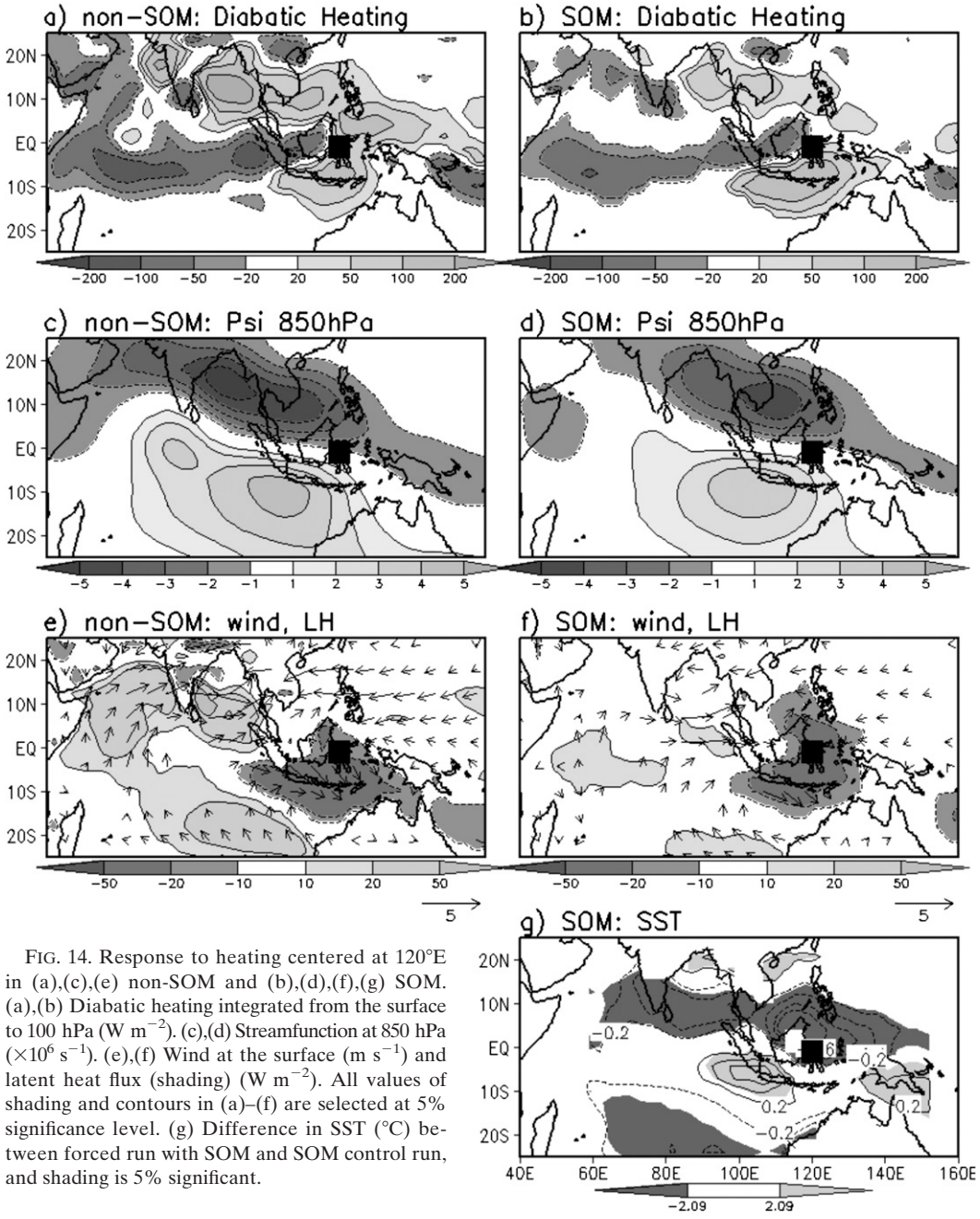

FIG. 14. Response to heating centered at 120°E in (a),(c),(e) non-SOM and (b),(d),(f),(g) SOM. (a),(b) Diabatic heating integrated from the surface to 100 hPa (W m^{-2}). (c),(d) Streamfunction at 850 hPa ($\times 10^6$ s^{-1}). (e),(f) Wind at the surface (m s^{-1}) and latent heat flux (shading) (W m^{-2}). All values of shading and contours in (a)–(f) are selected at 5% significance level. (g) Difference in SST (°C) between forced run with SOM and SOM control run, and shading is 5% significant.

experiments. In the SOM experiments, the two cyclonic centers to the west of the forcing are weaker and less extensive than in the non-SOM experiments. The maximum of the circulation is close to the forcing region in the SOM, while the maximum is over the Bay of Bengal in the non-SOM experiments. This is likely related to the strong response of the diabatic heating in the Bay of Bengal in the non-SOM experiments (Fig. 14a). For the heating over the warm ocean, the air–sea interaction induces a negative feedback between the additional diabatic heating and SST, thus altering the atmospheric circulation.

Negative diabatic heating responses are clearly seen over India for both heating (Fig. 14a) and cooling experiments (Fig. 15a). The negative response is expected in the case of inserted cooling over the western Pacific, but the negative response in the case of heating over the western Pacific (in Fig. 14a) is puzzling. The responses of

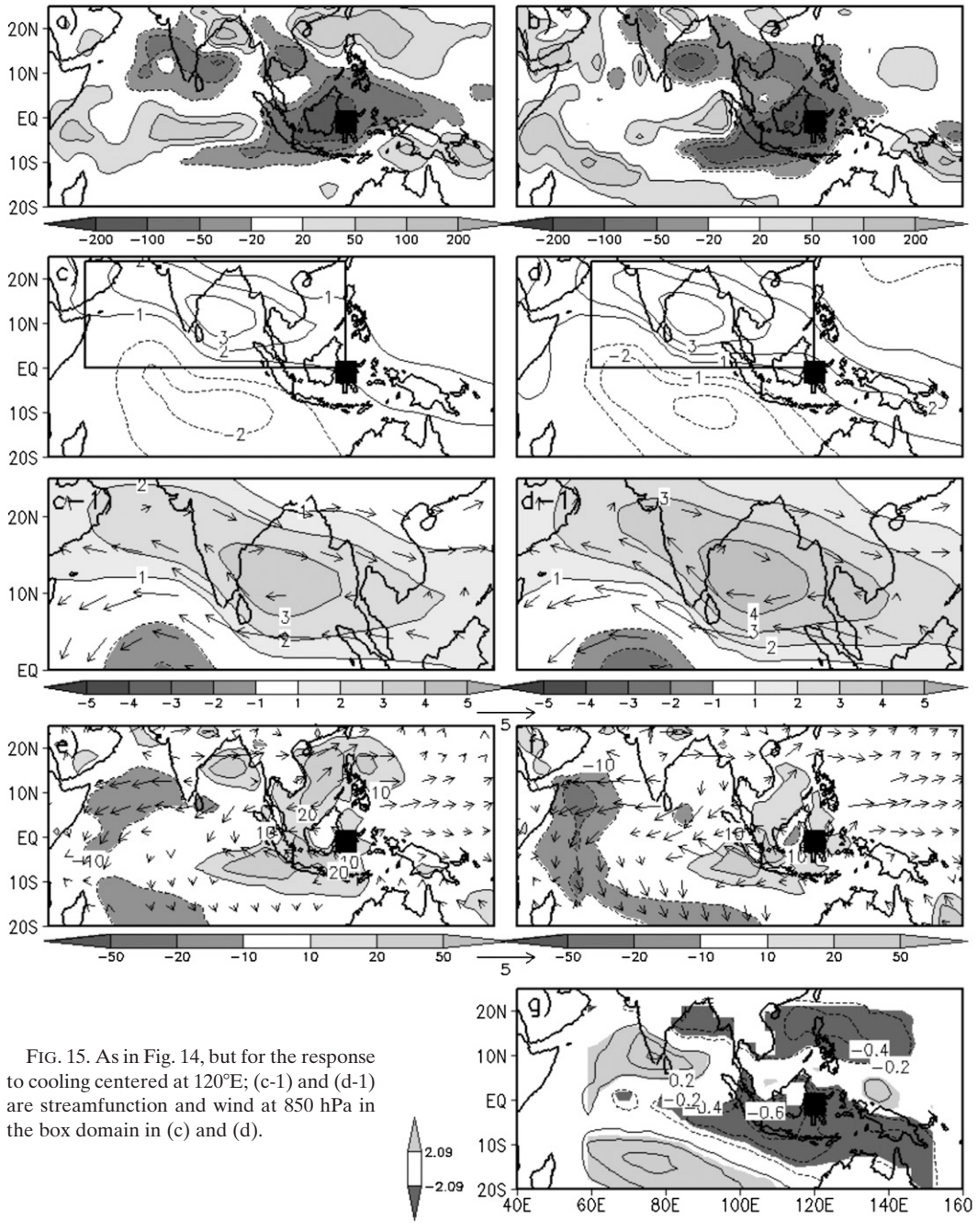

FIG. 15. As in Fig. 14, but for the response to cooling centered at 120°E; (c-1) and (d-1) are streamfunction and wind at 850 hPa in the box domain in (c) and (d).

divergence (integrated over 275–80 hPa) (Fig. 6c) and velocity potential at 200 hPa (Fig. 10e) show negative and positive anomalies over India, respectively, and so they are consistent with downward motion and suppressed convection. Since the heating over the western Pacific could be considered as a part of the La Niña forcing, the results of these heating experiments are not consistent with the general relationship between ENSO and the monsoon. This may be partly explained by the negative SST anomalies produced by regional air–sea coupling over the Maritime Continent and northern Indian Ocean, which are not observed.

2) COOLING EXPERIMENT

When the forcing (cooling) is centered at 120°E, the positive anomalies of the diabatic heating in the northwestern Pacific and the northern Bay of Bengal seen in the non-SOM (Fig. 15a) disappear in the SOM (Fig. 15b).

In the prescribed SST experiments, positive latent heat fluxes in these two regions are consistent with westerly wind anomalies (Fig. 15e). With air–sea interaction applied, the anomalies of latent heat flux (Fig. 15f) disappear and negative anomalies of SST (Fig. 15g) appear.

The streamfunction (Fig. 15d) shows an enhanced anticyclonic anomaly in the SOM experiments in the Indian Ocean to the west of Sumatra, as indicated by the box in Fig. 15d and a wider negative diabatic heating response over the western North Pacific (Fig. 15b). The responses of the latent heat flux in the non-SOM and SOM experiments are positive and similar in terms of the magnitudes in this region. In the SOM experiments, however, the positive latent heat flux decreases SST, leading to a further decrease in the diabatic heating anomalies. The air–sea interaction here, thus, contributes a positive feedback. Consistent with the stronger anticyclonic circulation, stronger easterlies (which add to the climatological easterlies in this region) are seen in Fig. 15f, thus increasing the magnitude of the wind.

The strengthened response by air–sea interaction agrees with the results of Wang et al. (2003): the anticyclonic circulations during El Niño summer are stronger than during the peak of El Niño because the air–sea interaction induces a positive feedback.

In addition, by applying SOM, positive diabatic heating anomalies over the equatorial Indian Ocean (Fig. 15a) almost disappear in the SOM experiment (Fig. 15b). Thus, the associated anomalous upward motion is also weakened, leading to a weaker anomaly in the Walker circulation.

In summary, in the heating experiments the air–sea interaction yields a negative feedback to the responses to the additional diabatic heating, with latent heat fluxes cooling the oceans in regions of added heating. In contrast, in the cooling experiments the air–sea interaction gives a positive feedback, with increased wind-induced latent heat flux leading to an enhancement of the anomalously cold SST, and enhanced downward motion. These feedbacks are tightly related to the monsoon flow. Thus, these feedbacks may change over the tropical central/eastern Pacific, where the mean surface zonal wind is easterly. In fact, the strong SST forcing over the tropical central and eastern Pacific mainly influences the atmosphere with little local atmospheric feedback (Lau and Nath 2000, 2003).

d. 1987 observed diabatic heating experiment

We ran an additional SOM experiment relevant for the summer of 1987. The inserted additional diabatic heating anomalies were chosen so that the *total* diabatic heating anomalies (additional heating plus model-generated heating) approximated the anomalous heating estimated from reanalyses for this period. The anomalous diabatic heating estimated from the reanalyses (Fig. 16a) shows the pattern of El Niño (cooling over the Maritime Continent and heating over the central–eastern Pacific) along with cooling over India, consistent with a dry monsoon. A pair of anomalous anticyclones over India and the Indian Ocean is seen in the observed streamfunction at 850 hPa (Fig. 16c) and velocity potential, and the divergent wind shows convergence over India and the western Pacific (Fig. 16d). The 1987 El Niño is a warm event that shows a clear anomalous atmospheric circulation consistent with the dry monsoon that was observed.

The additional heating (labeled as ''Forcing'' in Fig. 16) is based on the observed diabatic heating anomaly (labeled as ''QDB'' in Fig. 16) with the coefficients adjusted so that the total heating anomaly matches observations, as stated above. The AGCM's diabatic heating response to the forcing with SOM is shown in Fig. 17. A weakened monsoon (negative anomalies over India) is seen, along with a strengthened cooling and heating over the western and central/eastern Pacific. The total diabatic heating anomaly (Fig. 17b) has magnitudes over the Pacific comparable with the observed diabatic heating (Fig. 16a). The additional forcing induces an anomalous anticyclonic circulation and upper-level convergence over India (Figs. 17c,d), although the simulated anticyclonic circulation and divergent winds are stronger than the observed ones.

The western Pacific cooling as a part of the 1987 forcing is similar to the idealized cooling centered at 120°E. The anomalous anticyclonic responses at 850 hPa are the same for both experiments. However, while the upper-level convergence related to suppressed convection over India appears in both the observed diabatic heating experiment (Fig. 17d) and observation (Fig. 16d), the upper-level convergence does not appear in the idealized cooling experiment (Fig. 10d-1). In this 1987 case, the observed diabatic heating over the central–eastern Pacific might play an important role in suppressing convection over the Indian region. Watanabe and Jin (2003) also show that both the western Pacific cooling and central–eastern Pacific heating are necessary to simulate proper anticyclonic anomalies over the Indian region as El Niño related to low-level atmospheric circulation.

The same 1987 forcing is inserted in the model with the non-SOM. The diabatic heating response (Fig. 18a) again weakens the Indian monsoon and reinforces the additional heating (negative over the western Pacific and positive over the central Pacific). But strong positive anomalies now appear in the vicinity of India (Bay of Bengal and northwestern India) and the Philippines;

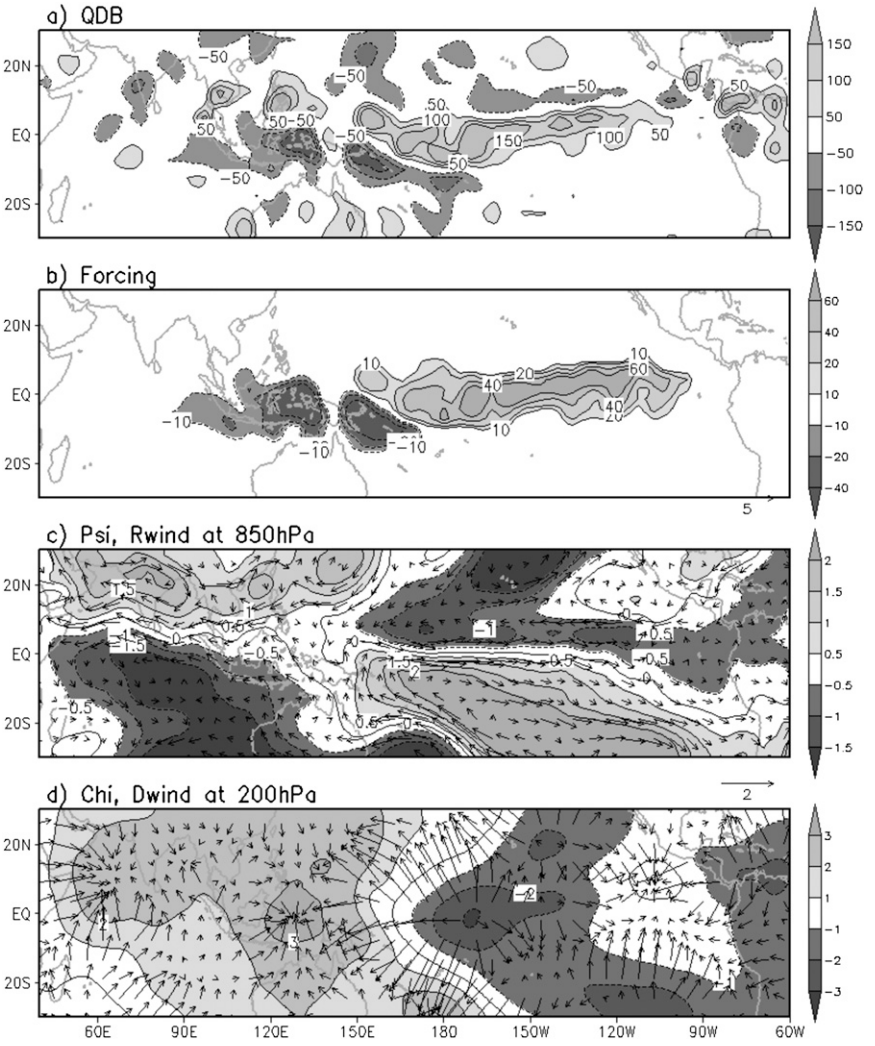

FIG. 16. (a) Vertically integrated anomalous diabatic heating (W m^{-2}) from the surface to 100 hPa during 1987 summer. (b) Forcing (W m^{-2}) for 1987 experiment. (c) Streamfunction at 850 hPa (shading, $\times 10^6$ s^{-1}) and rotational wind at 850 hPa (m s^{-1}) during 1987 summer. (d) Velocity potential (shading, $\times 10^6$ m^2 s^{-1}) and divergent wind (m s^{-1}) during 1987 summer.

anomalies that do not appear in the SOM experiment (Fig. 17a). In addition, an anomalous cyclonic circulation (Fig. 18c) is seen over the Bay of Bengal, and the anticyclonic circulation is shifted southward compared to the SOM. In the non-SOM experiment, there is no mechanism to allow the SST to cool in response to the increased latent heat supply to the atmosphere; hence, the Bay of Bengal and the Philippines experience increased diabatic heating.

6. Summary and discussion

The atmospheric response to the location of horizontally localized tropical diabatic heating anomalies is studied in CAM3, with particular reference to the Indian monsoon and its relationship to ENSO. We modify CAM3 by adding a relatively small diabatic heating with an idealized vertical structure and no time dependence in boreal summer integrations. The anomalous circulation forced by this added idealized heating influences the model's circulation, which in turn further changes the moist and radiative heating fields. Consideration of the ensemble mean response removes most of the effects of midlatitude disturbances.

This study of the sensitivity of the atmospheric response to the longitude of tropical heating in a full AGCM is more inclusive than a similar study using a simple dry model (Ting and Yu 1998) focused only on the dry dynamical response. Since the AGCM in this study includes moist and radiative processes, we are able

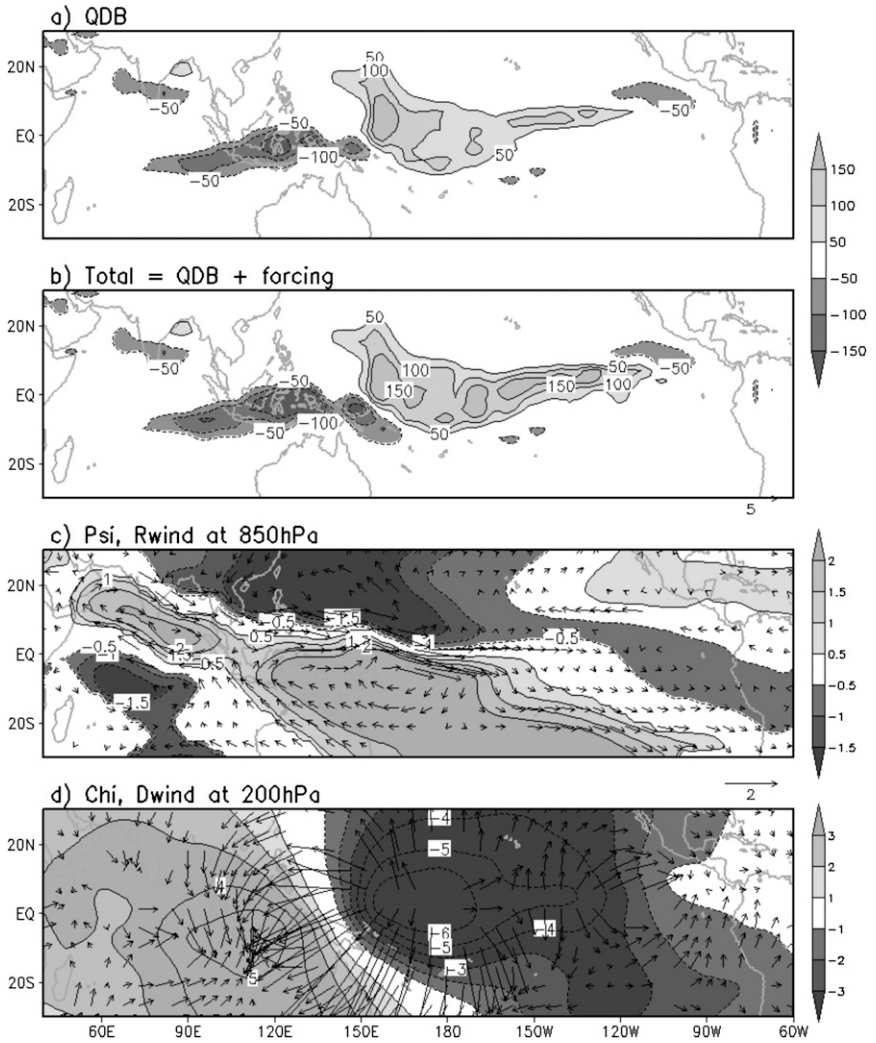

FIG. 17. Response to 1987 forcing with SOM. (a) Vertically integrated anomalous diabatic heating (W m^{-2}) from the surface to 100 hPa. (b) Sum of diabatic heating response and inserted forcing (W m^{-2}). (c) Streamfunction at 850 hPa ($\times 10^6$ s^{-1}) and rotational wind (m s^{-1}) at 850 hPa. (d) Velocity potential (shading, $\times 10^6$ m^2 s^{-1}) and divergent wind (m s^{-1}).

to assess the coupled response of the diabatic heating change and the atmospheric circulation change. The set of responses to the idealized forcing helps to understand the results of the forcing experiment relevant for the dry monsoon/El Niño case of 1987. This study and that of Jang and Straus (2012) are the first to apply the technique of additional heating in a full AGCM specifically to the case of the Indian monsoon.

Ting and Yu (1998) show the insensitivity of the atmospheric response to tropical forcing location in dry linear and nonlinear baroclinic models. In this study, the interaction between atmospheric response and diabatic heating leads differences. When the idealized heating/cooling is over the warm SST, there is an anchored response over the Bay of Bengal even as the idealized heating moves eastward. The anchored response extends to the Indian region, interacting with the monsoon flow. This anchored response disappears when the forcing is over cold SST (east of the date line). However, when the idealized forcing is over the eastern Pacific, there is a Kelvin wave–like response over the Indian region, which propagates eastward. Moreover, when the equatorial forcing is moved farther south to 7°S but still near the western Pacific, the response of the atmospheric circulation and diabatic heating over India becomes weak.

a. Role of heating/cooling near the Maritime Continent

When idealized cooling (nearly symmetric about the equator) is inserted near the Maritime Continent in the

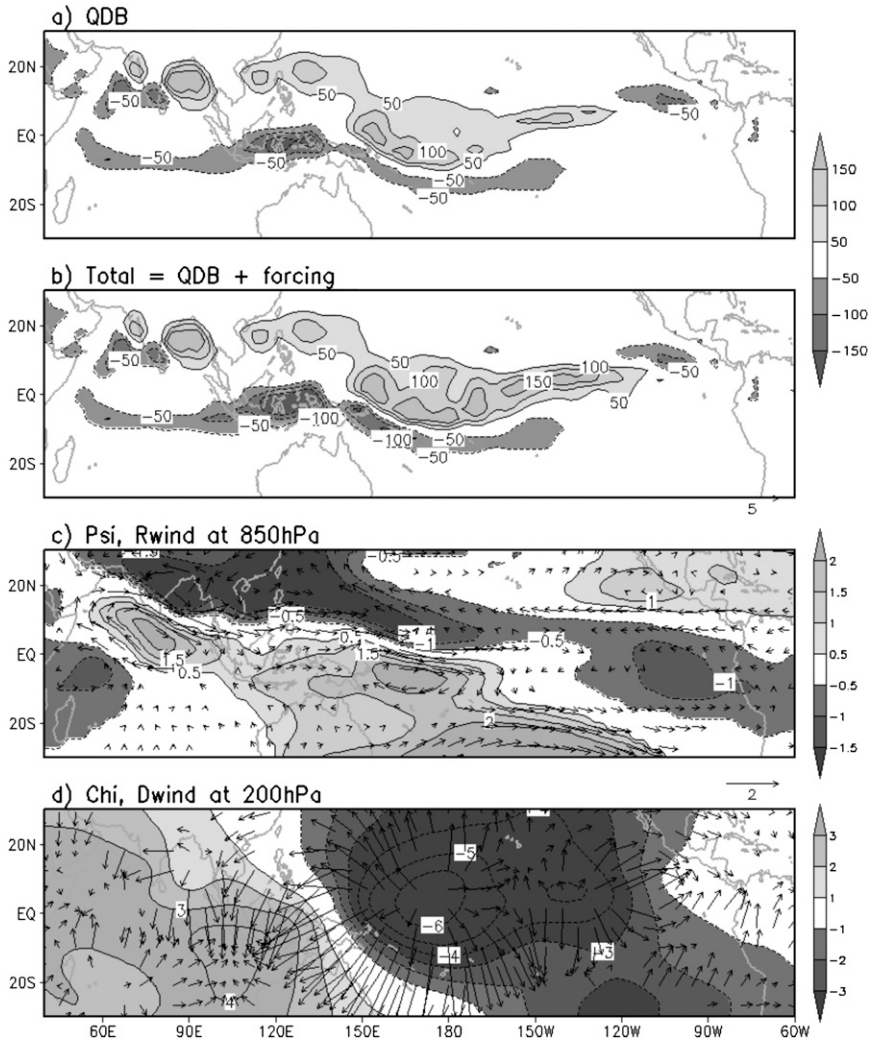

FIG. 18. As in Fig. 17, but for non-SOM.

model (appropriate for El Niño conditions), anomalous downward motion over the western Pacific is induced as well as an asymmetric Rossby wave response (anticyclonic circulation) to the west of the forcing, extending over the Indian region. Although the symmetric idealized cooling does not cover the Indian region, the asymmetric response shows that the downward motion branch of the anomalous Walker circulation can influence India.

The asymmetric Rossby response in a dry model is due to easterly vertical shear near the Indian region during northern summer (Wang et al. 2003; Xie and Wang 1996). The full AGCM experiments include the interaction between convection and equatorial waves. In this study, convergence near the surface helps to understand the asymmetric response. With the development of the Gill-type circulation, the low in surface pressure spreads to the north and south of the forcing region; the accompanying surface convergence leads to a meridionally and asymmetrically (stronger in the north) extended response of the diabatic heating. In Wu et al.'s (2006) symmetric (to the equator) propagating forcing (MJO like) experiment in an AGCM, the northward shift in precipitation is induced with the northward propagation of surface convergence.

b. Role of ocean–atmosphere coupling

Experiments with cooling in the western Pacific–Indonesian region (as in an El Niño event) show a positive feedback due to air–sea coupling related to latent heat flux and enhanced easterlies over Sumatra. The positive feedback is also emphasized as the reason for maintaining an anomalous circulation during the retreating phase of El Niño (Wang et al. 2000, 2003). In contrast,

when the heating is inserted in the Indonesian–western Pacific region, consistent with a La Niña event, a negative feedback is seen in the forced experiments. These different feedbacks are thought to be one of reasons for this asymmetric response between El Niño and La Niña.

In considering a real El Niño or La Niña event, the heating or cooling over a wide range of longitudes (including the far eastern Pacific and Indian Oceans) must be taken into account. In this study, the observed diabatic heating anomaly associated with one warm event (1987) is used to guide the additional heating to be added to the AGCM, so that the total AGCM heating anomaly resembles the observed. However, the observed estimate of heating is obtained from reanalysis fields, and thus it has some uncertainty associated with it, especially in data-poor areas. A better understanding of the possible errors in the estimated diabatic heating would be helpful in assessing these experiments. In addition, the AGCM used in this study has systematic errors over the monsoon areas and in the tropics in general; these certainly affect the results.

In the idealized experiments, heating over the far eastern Pacific may have an influence in the equatorial Indian Ocean (as suggested by Fig. 13), while the response over India to added heating over the Indian Ocean is opposite that of the same heating over Indonesia. It is also possible that the responses to anomalous heating in various regions interfere constructively or destructively. It remains to assemble the building blocks of the responses presented here to understand the monsoon response to the complex diabatic heating field associated with an observed ENSO. A step in that direction has been taken by Jang and Straus (2012).

Acknowledgments. We are grateful for discussions with Dr. J. Shukla. This work was supported by the National Science Foundation (Grants ATM-0830062 and ATM-0830068), the National Oceanic and Atmospheric Administration (Grant NA09 OAR4310058), the National Aeronautics and Space Administration (Grant NNX09AN50G), and the Office of Science (BER) of the U.S. Department of Energy (Grant DE-FG02-07ER64473). Computing support from the Climate Simulation Laboratory of the National Center for Atmospheric Research is also acknowledged.

APPENDIX A

Vertical Structure

The hybrid vertical coordinates are specified as input, and the corresponding midlayer pressures are calculated from these assuming a fixed surface pressure of $p_0 = 1000$ hPa. We use a standard set of $K = 26$ levels, with midlayer pressure values h_k as given in Table A1.

TABLE A1. Standard values (h_k) of midlevel pressure for hybrid coordinate system for CAM3.

Level K	Pressure (Pa)	Level K	Pressure (Pa)
1	354.5	14	22 651.3
2	739.9	15	26 648.1
3	1396.7	16	31 350.1
4	2394.5	17	36 881.8
5	3723.0	18	43 389.5
6	5311.5	19	51 045.5
7	7005.9	20	60 052.4
8	8543.9	21	69 679.6
9	10 051.5	22	78 770.2
10	11 825.0	23	86 716.1
11	13 911.5	24	92 964.9
12	16 366.2	25	97 055.5
13	19 254.0	26	99 255.6

For a profile to become very small at the bottom and top of the model, we use the following approximation ($1 \le k \le K$):

$$\hat{F}_k \approx \sum_{m=1}^{M} \left[A_m \cos\left(2\pi \frac{mk}{K}\right) + B_m \sin\left(2\pi \frac{mk}{K}\right) \right]. \quad \text{(A1)}$$

The values of A_m and B_m are given in Table A2 using $m = 2$. Equation (A1) is implemented in the CAM3 subroutine (dynamics and physics coupling module), in which the full temperature tendency is available in gridpoint configuration. The resulting profile is given by the blue dots in Fig. A1.

To achieve a somewhat shallower profile, we modify the formula in Eq. (A1) as shown:

$$F_k = \sin\left(\pi \frac{h_k}{p_0}\right) - 0.3 \sin\left(2\pi \frac{h_k}{p_0}\right) - 0.1 \sin\left(4\pi \frac{h_k}{p_0}\right). \quad \text{(A2)}$$

An extended heating is defined as above, and Fig. A1 shows this heating profile as the red dots.

TABLE A2. Coefficients of A_m and B_m; $m = 2$, harmonic coefficients correspond to heating of Eq. (A1).

	$m = 1$	$m = 2$
A_m	−0.0418	−0.0392
B_m	−0.6917	−0.3230

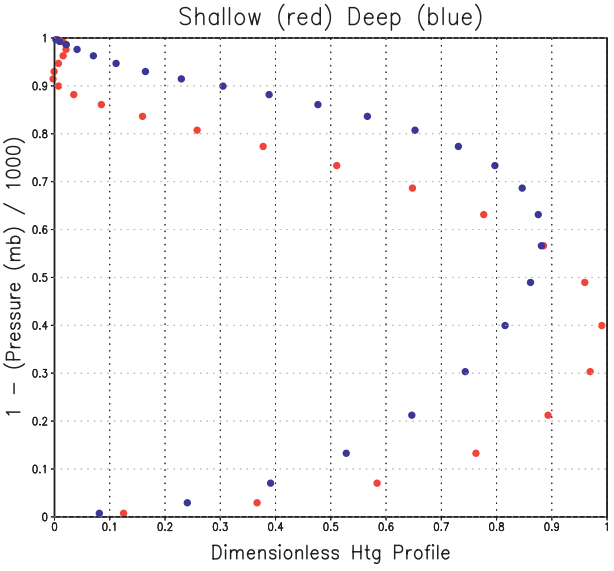

FIG. A1. Heating profiles derived by harmonic approximation. See the text for details.

To compare the two profiles with observed diabatic heating, the vertical structure of anomalous diabatic heating fields obtained from ERA-40 data by Nigam et al. (2000) is shown for El Niño and La Niña events in Fig. A2. Two types of the vertical structures are shown: those for a single grid point (2.5°S, 132°E; solid lines with closed circles) and one for spatially averaged values (5°S–2°N, 120°–140°E; dashed lines). In Fig. A1, the shallow vertical profiles show a maximum at 600 mb and the deep profiles show a maximum at about 450 mb. ERA-40 diabatic heating for both El Niño and La Niña shows the maximum below 500 mb, although each event has a somewhat different vertical structure. In all the experiments in this paper, the shallower profile (red dots in Fig. A1) is used for the vertical structure.

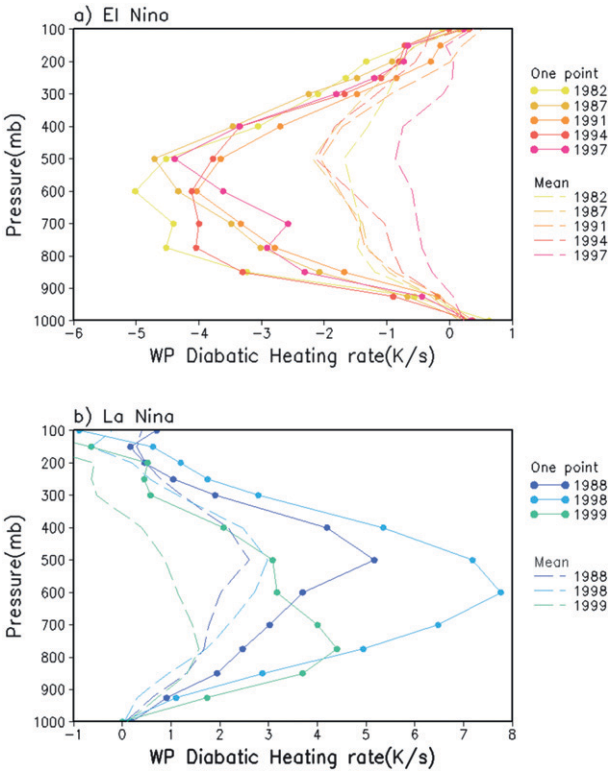

FIG. A2. Vertical structure of ERA-40 diabatic heating rate (K s^{-1}). (a) For El Niño event (1982, 1987, 1991, 1994, and 1997). The solid lines with closed circles are at 2.5°S, 132°E. The dashed lines are averaged from 5°S to 2°N and from 120° to 140°E. (b) For La Niña (1988, 1998, and 1999). The solid lines with closed circles are at 2.5°S, 137°E for 1988, and at 2.5°S, 100°E for 1998 and 1999. For 1988 the dashed lines are averaged from 5°S to 2°N and from 130° to 140°E, and are averaged from 5°S to 2°N and from 95° to 105°E for 1998 and 1999.

Note that since we have assumed the surface pressure to be equal to p_0, the coordinate in Fig. A1 should really be the model coordinate; the correspondence with pressure is only valid if the true surface pressure is close to p_0, typically over the ocean.

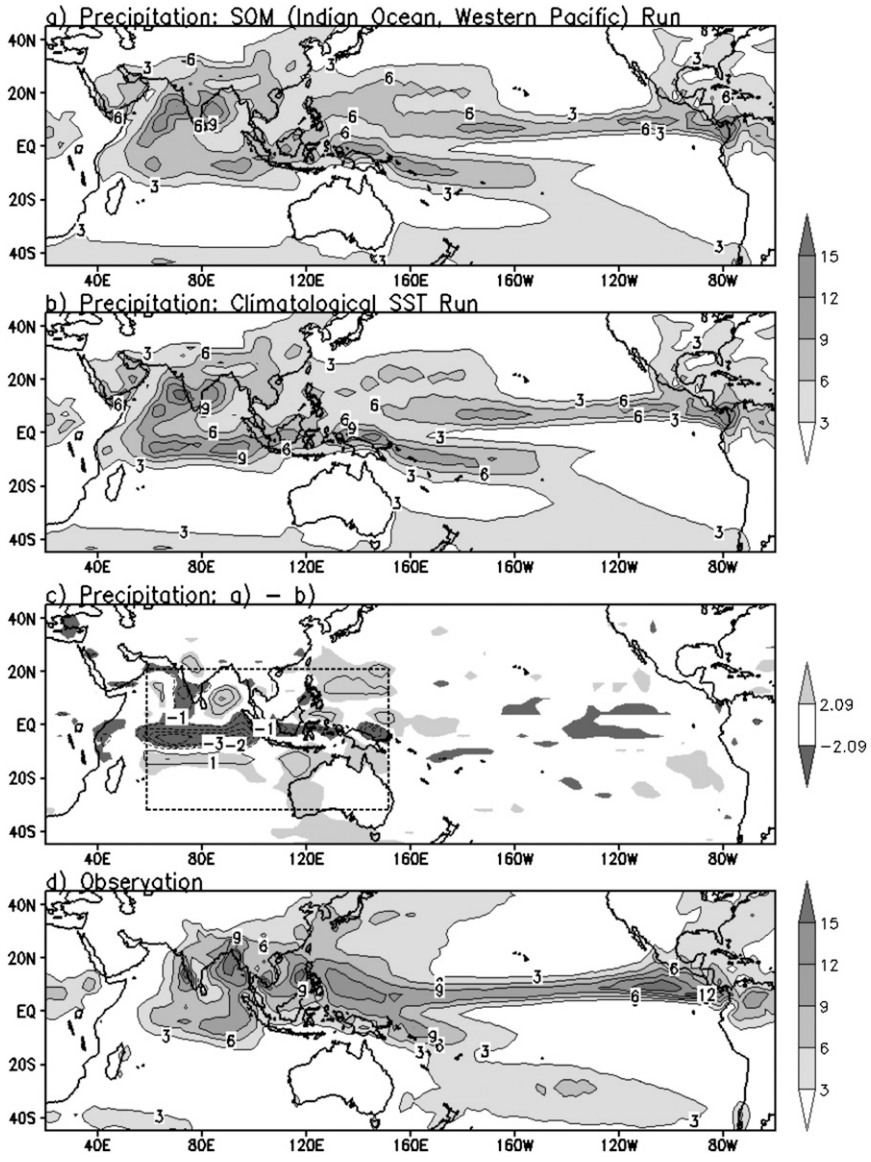

FIG. B1. Mean precipitation (mm day^{-1}) during northern summer (May–August). (a) Control run with an SOM over the Indian Ocean and western Pacific. (b) Control run with climatological SST. (c) Differences between (a) and (b). Shading is at 5% significance, and box is the SOM domain. (d) Observed precipitation.

APPENDIX B

Comparison of Control Runs: Effect of SOM

We briefly compare the boreal summer mean state from the two control runs. The mean precipitation of the CCTL (non-SOM) has excessively large precipitation over the equatorial Indian Ocean compared to the observed precipitation (see Fig. B1d). In Fu et al. (2002), excessive rainfall over the equatorial Indian Ocean is also mentioned as a common problem of AGCMs. The magnitude of the precipitation in the SOM control run (Fig. B1a) over the Indian Ocean is more similar to observations. In Fu et al. (2002) and Wu and Kirtman (2005), excessive precipitation over the equatorial Indian Ocean is reduced by applying the regional air–sea coupling. However, the simulated precipitation over the Maritime Continent and along the Somali coast is still large compared to observations, while the precipitation is underestimated over the Bay of Bengal and in the vicinity of the Philippines (including the western Pacific and South China Sea).

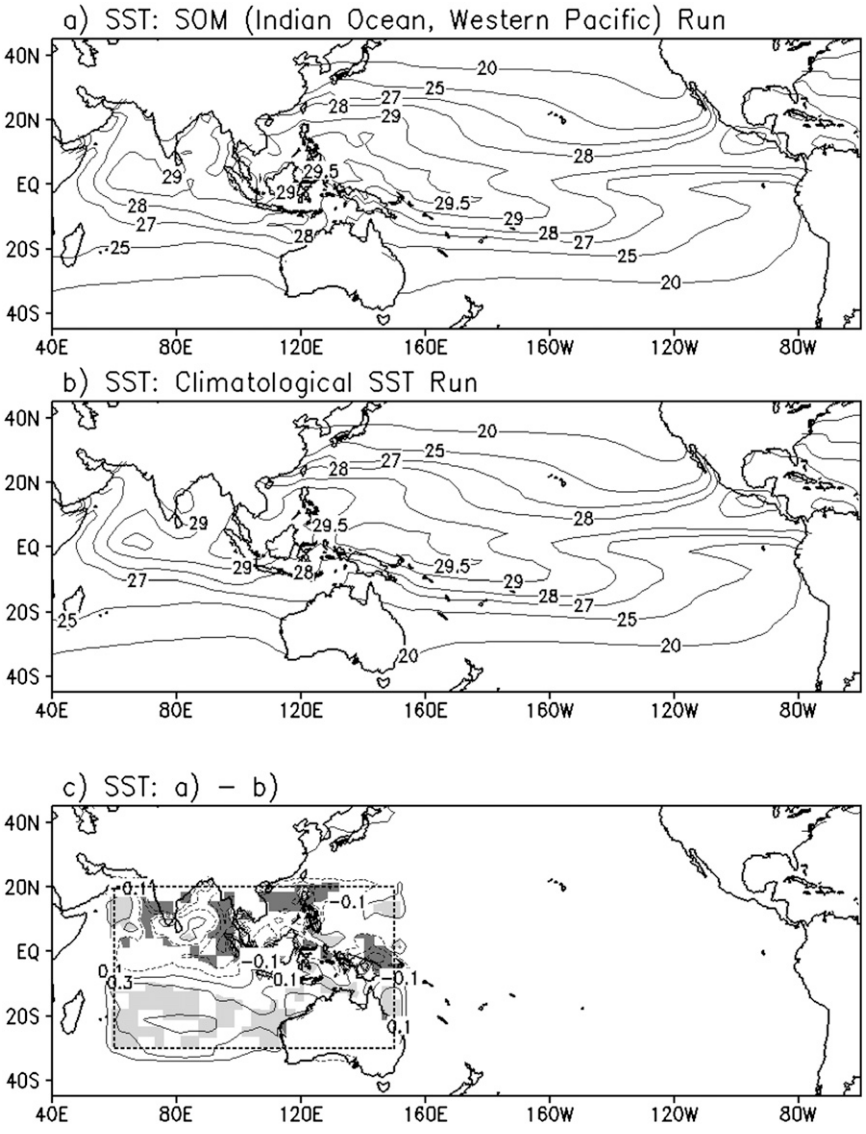

FIG. B2. Mean SST (°C) during northern summer (May–August). (a) Second control run with an SOM over the Indian Ocean and western Pacific. (b) Control run with climatological SST. (c) Differences between (a) and (b), and shading is at 5% significance; box is the SOM domain.

For the CTL SOM, negative anomalies (differences) of SST compared to CCTL appear over the northern portion of the Indian Ocean where there is large precipitation. As in Wu and Kirtman (2005), this represents a negative feedback in which a reduction of incoming solar radiation by cloudiness associated with convection near India cools the ocean (Fig. B2c), and reduces the precipitation (Fig. B1c). Enhanced westerlies near the surface over the equatorial Indian Ocean (Fig. B3) are also related to the reduced precipitation. The increased wind induces latent heat flux from the ocean to the atmosphere, thereby lowering the SST. So, anomalously negative SST may reduce precipitation or the released latent heat flux supply heating to existing clouds as enhancing precipitation. In the lead–lag correlation analysis (not shown), when the SST leads rain by 1 month, the correlation is larger than between rain and latent heat flux. We thus hypothesize that decreased SST (due to increased westerlies) contributes to reduced precipitation over the equatorial Indian Ocean. However, in the southern portion of the Indian Ocean, positive anomalies of SST appear (Fig. B2c)—here, different feedbacks between the ocean and atmosphere operate.

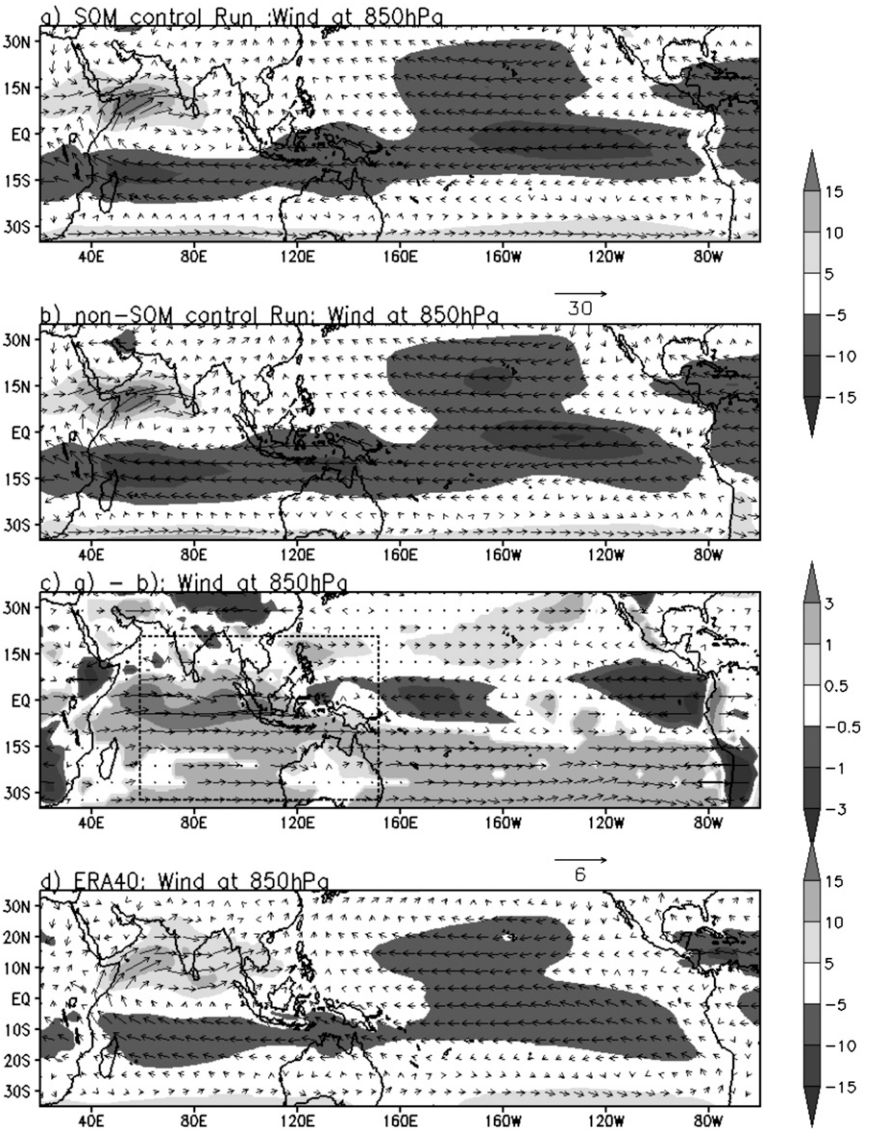

FIG. B3. Mean wind (m s^{-1}) during northern summer (May–August). Shading indicates the zonal wind in (a) control run with an SOM over the Indian Ocean and western Pacific, (b) control run with climatological SST, and (d) observed wind (ERA-40). (c) Differences between (a) and (b), and the zonal wind at 5% significance are selected and shaded; box is the SOM domain.

The observed mean summer flow at 850 hPa is easterly over the southern Indian Ocean. Toward South Africa the flow turns northward and becomes westerly (Somalia jet) (Fig. B3d). These main features also appear in the two control runs (Figs. B3a,b). However, in the model the westerlies to the west of India and the easterlies over the southern portion of the Indian Ocean are too strong, while the westerly flow in the Bay of Bengal and the South China Sea is too weak. By applying the SOM regionally, the excessively strong easterly flow over the southern Indian Ocean becomes weaker (cf. Figs. B3a,b) but still large compared to observation.

The systematic errors in the model, such as overly strong easterlies over the Indian Ocean and errors in precipitation in the vicinity of India, may influence the results of the experiments in this study.

REFERENCES

Annamalai, H., 2010: Moist dynamical linkage between the equatorial Indian Ocean and the South Asian monsoon trough. *J. Atmos. Sci.,* **67,** 589–610.

Barsugli, J. J., and P. D. Sardeshmukh, 2002: Global atmospheric sensitivity to tropical SST anomalies throughout the Indo-Pacific basin. *J. Climate,* **15,** 3427–3442.

Branstator, G., 1985: Analysis of general circulation model sea-surface temperature anomaly simulations using a linear model. Part I: Forced solutions. *J. Atmos. Sci.,* **42,** 2225–2241.

Chan, S. C., and S. Nigam, 2009: Residual diagnosis of diabatic heating from ERA-40 and NCEP reanalyses: Intercomparisons with TRMM. *J. Climate,* **22,** 414–428.

Collins, W. D., and Coauthors, 2006: The formulation and atmospheric simulation of the Community Atmosphere Model Version 3 (CAM3). *J. Climate,* **19,** 2144–2161.

Fu, X., B. Wang, and T. Li, 2002: Impacts of air–sea coupling on the simulation of mean Asian summer monsoon in the ECHAM4 model. *Mon. Wea. Rev.,* **130,** 2889–2904.

Gill, A. E., 1980: Some simple solutions for heat-induced tropical circulation. *Quart. J. Roy. Meteor. Soc.,* **106,** 447–462.

Jang, Y., and D. M. Straus, 2012: The Indian monsoon circulation response to El Niño diabatic heating. *J. Climate,* **25,** 7487–7508.

Keshavamurthy, R. N., 1982: Response of the atmosphere to sea surface temperature anomalies over the equatorial Pacific and the teleconnections of the Southern Oscillation. *J. Atmos. Sci.,* **39,** 1241–1259.

Kirtman, B. P., and J. Shukla, 2000: Influence of the Indian summer monsoon on ENSO. *Quart. J. Roy. Meteor. Soc.,* **126,** 213–239.

Kripalani, R. H., and A. Kulkarni, 1997: Climate impacts of El Niño/La Niña on the Indian monsoon: A new perspective. *Weather,* **52,** 39–46.

Kumar, K. K., B. Rajagopalan, and M. A. Cane, 1999: On the weakening relationship between the Indian monsoon and ENSO. *Science,* **284,** 2156–2159.

Lappen, C.-L., and C. Schumacher, 2012: Heating in the tropical atmosphere: What level of detail is critical for accurate MJO simulations in GCMs? *Climate Dyn.,* **39,** 2547–2568.

Lau, N.-C., and M. J. Nath, 2000: Impact of ENSO on the variability of the Asian–Australian monsoons as simulated in GCM experiments. *J. Climate,* **13,** 4287–4309.

——, and ——, 2003: Atmosphere–ocean variations in the Indo-Pacific sector during ENSO episodes. *J. Climate,* **16,** 3–20.

Lin, H., J. Derome, and G. Brunet, 2007: The nonlinear transient atmospheric response to tropical forcing. *J. Climate,* **20,** 5642–5665.

Lindzen, R. S., and S. Nigam, 1987: On the role of sea surface temperature gradients in forcing low-level winds and convergence in the tropics. *J. Atmos. Sci.,* **44,** 2418–2436.

Meehl, G. A., J. M. Arblaster, and G. Branstator, 2008: A coupled air–sea response mechanism to solar forcing in the Pacific region. *J. Climate,* **21,** 2883–2897.

Mokhov, I. I., D. A. Smirnov, P. I. Nakonechny, S. S. Kozlenko, E. P. Seleznev, and J. Kurths, 2011: Alternating mutual influence of El-Niño/Southern Oscillation and Indian monsoon. *Geophys. Res. Lett.,* **38,** L00F04, doi:10.1029/2010GL045932.

Nigam, S., C. Chung, and E. DeWeaver, 2000: ENSO diabatic heating in ECMWF and NCEP–NCAR reanalyses, and NCAR CCM3 simulation. *J. Climate,* **13,** 3152–3171.

Palmer, T. N., C. Brankovic, P. Viterbo, and M. J. Miller, 1992: Modeling interannual variations of summer monsoons. *J. Climate,* **5,** 399–417.

Pillai, P. A., and H. Annamalai, 2012: Moist dynamics of severe monsoons over South Asia: Role of the tropical SST. *J. Atmos. Sci.,* **69,** 97–115.

Raymond, J. D., 1994: Convective processes and tropical atmospheric circulation. *Quart. J. Roy. Meteor. Soc.,* **120,** 1431–1455.

Reynolds, R. W., N. A. Rayner, T. M. Smith, D. C. Stokes, and W. Wang, 2002: An improved in situ and satellite SST analysis for climate. *J. Climate,* **15,** 1609–1625.

Sardeshmukh, P. D., and B. J. Hoskins, 1988: The generation of global rotational flow by steady idealized tropical divergence. *J. Atmos. Sci.,* **45,** 1228–1251.

Slingo, J. M., and H. Annamalai, 2000: 1997: The El Niño of the century and the response of the Indian summer monsoon. *Mon. Wea. Rev.,* **128,** 1778–1797.

Straus, D. M., and V. Krishnamurthy, 2007: The preferred structure of the interannual Indian monsoon variability. *Pure Appl. Geophys.,* **164,** 1717–1732.

Ting, M., and L. Yu, 1998: Steady response to tropical heating in wavy linear and nonlinear baroclinic models. *J. Atmos. Sci.,* **55,** 3565–3582.

Troup, A. J., 1965: Southern Oscillation. *Quart. J. Roy. Meteor. Soc.,* **91,** 490–506.

Wang, B., R. Wu, and X. Fu, 2000: Pacific–East Asian teleconnection: How does ENSO affect East Asian climate? *J. Climate,* **13,** 1517–1536.

——, ——, and T. Li, 2003: Atmosphere–warm ocean interaction and its impacts on Asian–Australian monsoon variation. *J. Climate,* **16,** 1195–1211.

Watanabe, M., and F.-F. Jin, 2003: A moist linear baroclinic model: Coupled dynamical–convective response to El Niño. *J. Climate,* **16,** 1121–1139.

Webster, P. J., V. O. Magaña, T. N. Palmer, J. Shukla, R. A. Tomas, M. Yanai, and T. Yasunari, 1998: Monsoon: Processes, predictability, and the prospects for prediction. *J. Geophys. Res.,* **103** (C7), 14 451–14 510.

Wu, M.-L. C., S. D. Schubert, M. J. Suarez, P. J. Pegion, and D. E. Waliser, 2006: Seasonality and meridional propagation of MJO. *J. Climate,* **19,** 1901–1921.

Wu, R., and B. P. Kirtman, 2005: Roles of Indian and Pacific Ocean air–sea coupling in tropical atmospheric variability. *Climate Dyn.,* **25,** 155–170.

Xie, P., and P. A. Arkin, 1997: Global precipitation: A 17-year monthly analysis based on gauge observations, satellite estimates, and numerical model outputs. *Bull. Amer. Meteor. Soc.,* **78,** 2539–2558.

Xie, X., and B. Wang, 1996: Low-frequency waves in vertically sheared zonal flow. Part II: Unstable waves. *J. Atmos. Sci.,* **53,** 3589–3605.